Icarus 226 (2013) 1020–1037

Contents lists available at ScienceDirect

Icarus

journal homepage: www.elsevier.com/locate/icarus

Saturn's visible lightning, its radio emissions, and the structure of the 2009–2011 lightning storms ☆

Ulyana A. Dyudina [a,*], Andrew P. Ingersoll [a], Shawn P. Ewald [a], Carolyn C. Porco [b], Georg Fischer [c], Yoav Yair [d]

[a] Division of Geological and Planetary Sciences, California Institute of Technology, 150-21, Pasadena, CA 91125, USA
[b] Cassini Imaging Central Laboratory for Operations, Space Science Institute, 4750 Walnut Street, Suite 205, Boulder, CO 80301, USA
[c] Space Research Institute, Austrian Academy of Sciences, Schmiedlstr. 6, A-8042 Graz, Austria
[d] The Open University of Israel, 1 University Road, Ra'anana 43107, Israel

ARTICLE INFO

Article history:
Received 19 March 2013
Revised 17 June 2013
Accepted 6 July 2013
Available online 20 July 2013

Keywords:
Saturn, Atmosphere
Atmospheres, Dynamics
Image processing
Lightning
Saturn

ABSTRACT

Visible lightning on Saturn was first detected by the Cassini camera in 2009 at ~35° South latitude. We report more lightning observations at ~35° South later in 2009, and lightning in the 2010–2011 giant lightning storm at ~35° North. The 2009 lightning is detected on the night side of Saturn in a broadband clear filter. The 2011 lightning is detected on the day side in blue wavelengths only. In other wavelengths the 2011 images lacked sensitivity to detect lightning, which leaves the lightning spectrum unknown.

The prominent clouds at the west edge, or the "head" of the 2010–2011 storm periodically spawn large anticyclones, which drift off to the east with a longitude spacing of 10–15° (~10,000 km). The wavy boundary of the storm's envelope drifts with the anticyclones. The relative vorticity of the anticyclones ranges up to $-f/3$, where f is the planetary vorticity. The lightning occurs in the diagonal gaps between the large anticyclones. The vorticity of the gaps is cyclonic, and the atmosphere there is clear down to level of the deep clouds. In these respects, the diagonal gaps resemble the jovian belts, which are the principal sites of jovian lightning.

The size of the flash-illuminated cloud tops is similar to previous detections, with diameter ~200 km. This suggests that all lightning on Saturn is generated at similar depths, ~125–250 km below the cloud tops, probably in the water clouds. Optical energies of individual flashes for both southern storms and the giant storm range up to 8×10^9 J, which is larger than the previous 2009 equinox estimate of 1.7×10^9 J. Cassini radio measurements at 1–16 MHz suggest that, assuming lightning radio emissions range up to 10 GHz, lightning radio energies are of the same order of magnitude as the optical energies.

Southern storms flash at a rate ~1–2 per minute. The 2011 storm flashes hundreds of times more often, ~5 times per second, and produces $\sim 10^{10}$ W of optical power. Based on this power, the storm's total convective power is of the order 10^{17} W, which is uncertain by at least an order of magnitude, and probably is underestimated. This power is similar to Saturn's global internal power radiated to space. It suggests that storms like the 2010–2011 giant storm are important players in Saturn's cooling and thermal evolution.

1. Introduction

Lightning on Saturn was first, controversially, detected by the Voyagers as radio emissions called Saturn Electrostatic Discharges, or SEDs (Burns et al., 1983; Kaiser et al., 1983; Yair et al., 2008). The lightning origin of SEDs was later confirmed by Cassini using correlation of SEDs with convective-looking clouds in the images (Porco et al., 2005; Fischer et al., 2007; Dyudina et al., 2007). The first direct observation of lightning flashes in Cassini night side images was taken during Saturn's 2009 equinox (Dyudina et al., 2010). Equinox geometry minimizes ring light illuminating Saturn's clouds, which is the main obstacle for lightning detection. The lightning flashes were detected at planetocentric latitudes of ~−35°, where most of the lightning storm clouds were seen, and where the SEDs were observed by Cassini since its arrival at Saturn in 2004. These thunderstorms occurred one at a time, lasting for days to months, and had months to years of lightning-free gaps in between (Fischer et al., 2011b). The optical lightning observations at equinox were luckily taken during an active storm, the longest of the detected thunderstorms, which lasted from mid-January to mid-December 2009.

This paper reports on new detections of visible lightning by the Cassini camera obtained after the equinox. This includes more

* Corresponding author. Fax: +1 626 585 1917.
E-mail address: ulyana@gps.caltech.edu (U.A. Dyudina).

0019-1035/$ - see front matter © 2013 The Authors. Published by Elsevier Inc. All rights reserved.
http://dx.doi.org/10.1016/j.icarus.2013.07.013

flashes detected in the 2009 storm and the flashes in the sunlit clouds of the 2010–2011 north hemisphere's giant storm. The 2010–2011 detection is the first observation of lightning on the day side of any planet other than the Earth. The 2010–2011 giant storm (Fischer et al., 2011a; Sánchez-Lavega et al., 2011; Fletcher et al., 2011; Sayanagi et al., 2013; Laraia et al., 2013; Janssen et al., 2013; García-Melendo et al., 2013) is much larger than the 2004–2009 southern storms and is usually classified as one of the Great White Spots, which are planet-encircling storms that occur about once every Saturn's year (29.5 Earth years) (Sánchez-Lavega et al., 2011). In this paper we give new estimates of the energies, rates, and location of Saturn's lightning, related structure and dynamics of the storms, and relations between visible lightning and SEDs.

Section 2 shows how the new lightning observations, detecting Saturn's lightning on the cloud background for the first time, reveal the exact location of lightning within the cloud. We derive wind vectors, vorticity, and cloud heights of the 2010–2011 storm on February 26 2011, at the time of the lightning observations. Also we relate lightning to cloud motions. In Section 3 we infer the vertical location (depth) of lightning using the observed lightning spot size. Section 4 reports timing of the flashes on timescales down to the fraction of a second and their relation to SEDs. Section 5 presents energies and flash rates of lightning, their statistical relation with SEDs, power produced by the 2010–2011 giant storm and its importance for Saturn's thermal evolution. Section 6 discusses why the detection of visible lightning in blue-filtered images and not in other wavelengths cannot be used to infer the lightning color. In other words, we cannot say that the lightning is blue. We discuss the relation of clouds to lightning, and the detectability of lightning by radio and imaging on the day and night sides of Saturn in Section 7.

Some additional details on the lightning flash data, and the techniques used for lightning detection and wind measurement are described in the Appendix A.

2. Lightning geometry and cloud motion

Optical lightning was first detected on the night side of Saturn during the August 2009 equinox (Dyudina et al., 2010). At equinox the ring illumination of Saturn was minimal, and the clouds were not seen. Over 12 min of observations, the lightning flashes were consistent with a single location at $-36.4^\circ \pm 0.1^\circ$ planetocentric latitude producing flashes about once a minute. We will use planetocentric latitudes for the rest of the paper.

Fig. 1 shows another night side detection in 2009, also at about -35° latitude, with lightning flashes in a cloud illuminated by Saturn's rings. Unlike the single-location equinox observations, during the 16 min of observation this storm flashes at least in two locations. The exposure times of the images in Fig. 1 alternate between 120 s and 15 s (see also Table A1 of the Appendix A). The two different exposure levels can be distinguished by the smear of the cloud boundaries induced by Saturn's rotation in 120-s exposures. From the five 15-s exposures (total 75 s), two showing lightning, we infer a rate of 1–2 flashes per minute. Accordingly, 2–4 such flashes would be expected during each of the 120-s exposures. They are hard to identify. Most likely those flashes are seen in each of the long-exposure images as faint spots not substantially exceeding the background brightness (which accumulates with exposure length). In addition, there are three bright flashes in the 120-s frames 4 and 8. These flashes have round shapes in map projection, are not smeared, and therefore are probably bright single flashes that occur rarely (see timing discussion in Section 4).

Fig. 2 shows locations of the flashes seen on Saturn's day side in the giant storm on February 26 2011. The background false-color map shows clouds at different depths by different colors: blue indicates upper haze, green – intermediate clouds, red – deep clouds, and white – optically thick clouds reaching the upper levels of the atmosphere.

Several locations of the storm flash repeatedly during the two Saturn days, i.e., flashes appear at nearly the same place in the two maps in Fig. 2. Lightning is most active near the head of the storm. Three flashes are detected there: two in the first map (double yellow $\times$ symbol), and one in the second map. Radio observations show that the head was producing most of the lightning throughout the storm's life (Fischer et al., 2011a; Sayanagi et al., 2013).

As predicted from the radio data in Fischer et al. (2011a), lightning occurred not just near the head, but also in other locations in the storm. SEDs were observed over an increasing longitudinal range as the storm grew, indicating lightning between the head and the large blue anticyclonic vortex at the right edge of Fig. 2). SED measurements show that at the end of February lightning flashes occurred over $\sim 80^\circ$ of longitude eastward from the head. Optical flashes in Fig. 2 are spread over $\sim 70^\circ$ in longitude. This is about 2/3 of the distance from the head to the vortex. The last 1/3 of the storm (longitudes 0° to 40° in Fig. 2) has a less turbulent appearance than the first 2/3. Possibly the weaker updrafts are manifested in less efficient charge generation and separation processes, which eventually lead to weaker electrical fields and fewer (or none at all) flashes.

Figs. 3–5 show the details of Fig. 2 at higher spatial resolution (see Online Supplemental Data for even higher resolution versions), and velocity and vorticity maps. Our cloud-tracking technique for measuring velocity and vorticity and the uncertainties are described in detail in the Appendix A.

As one can see from Figs. 3–5, there are many regions with vorticity more negative than $-5 \times 10^{-5}\,s^{-1}$. These are large anticyclones, which dominate the flow field within the storm. The head itself is a large anticyclone, and it seems to shed anticyclones that drift off downstream to the east. The blue oval at longitudes 350–360° west (Fig. 5) is the first anticyclone; it was shed in December 2010, shortly after the storm appeared (Sánchez-Lavega et al., 2011; Sayanagi et al., 2013). The head sheds these anticyclones at a nearly constant rate, so the spacing between them remains roughly constant (Sayanagi et al., 2013) in the range 10–15° of longitude ($\sim$8500–13,000 km). The clouds that mark the northern edge of the storm have a wave-like appearance. The crests and troughs of the wave are associated with the anticyclones and move with them to the east, away from the source. The crests and troughs are not standing waves, like ship waves or waves behind boulders in a stream, whose phase speed matches that of their source. In other words, they are not simple Rossby waves propagating to the west with the head.

Strictly speaking, Figs. 3–5 show maps of relative vorticity ζ, the spin of fluid elements due to their motion relative to the planet. The largest negative values in the Saturn storm are probably about $-7 \times 10^{-5}\,s^{-1}$, although even larger values may have been obscured during smoothing of the vorticity map. The other element of vorticity is the planetary vorticity f, which arises due to the rotation of the planet. At the latitude of the storm, this planetary vorticity $f = 2\Omega sin\,\phi_g$ is $20 \times 10^{-5}\,s^{-1}$, where ϕ_g is planetographic latitude. Thus the relative vorticity is of order $-f/3$, which is 1/3 of the limiting value $-f$ of an anticyclone under gradient wind balance (Salby, 1996; Holton, 2004). Fluid elements emerge from the adiabatic fluid interior of the planet with zero values of Ertel's potential vorticity Q, since Q is proportional to the gradient of potential temperature and that is zero for an adiabatic region (Salby, 1996; Holton, 2004). As they emerge into the stably stratified troposphere, the fluid elements still have $Q \approx 0$, because Q is a conserved quantity, but they accomplish this by

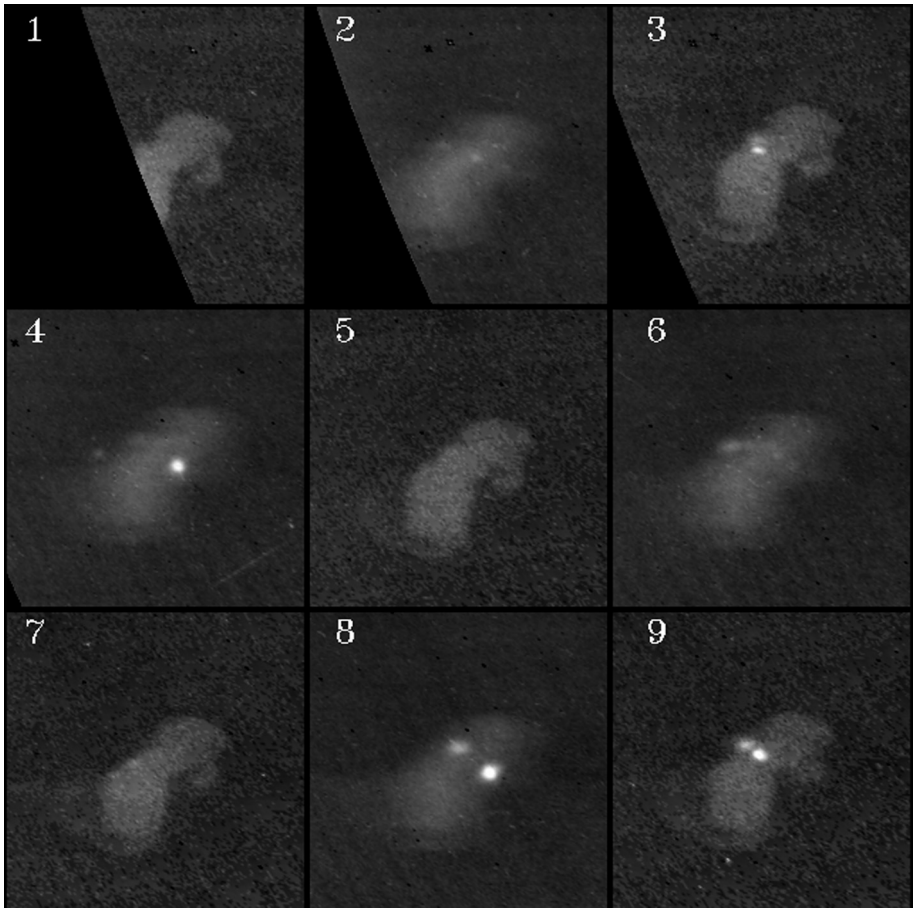

Fig. 1. Lightning flashing on the night side of Saturn at planetocentric latitude ~−35° (see flash locations in Table A1 of the Appendix A). The nine repeated images of the same area are taken during 16 min on November 30, 2009 (see timing in Section 4 and the Appendix A). The map-projected images are shown in chronological order following the panels' number. The exposure times are 15 s for frames 1, 3, 5, 7, 9 and 120 s for frames 2, 4, 6, 8. The pale gray ~3000-km-long cloud is illuminated by light from Saturn's rings and does not change during the observation. The bright spots are the lightning flashes, which occured in some of the frames but not in others. The images have been processed so that the gray cloud has the same brightness in all the images. An animated version of this data combined with sound from the radio data can be found in the paper's Online Supplementary Data.

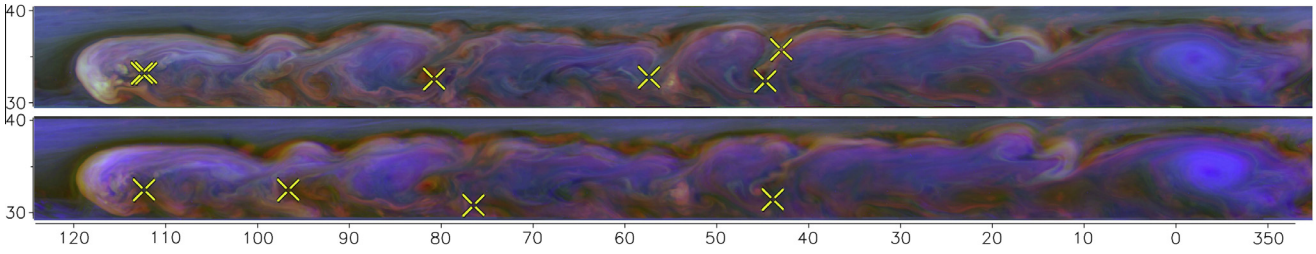

Fig. 2. Lightning locations in the 2010–2011 giant storm on Saturn on the methane band mosaic of the storm clouds. The lightning detected with the blue filter are shown by yellow open-center × symbols on the background of a false-color map composed from three methane band filters. For filter shapes see Fig. 11 and Porco et al. (2004). These three filters are sensitive to different amounts of absorption by methane gas. The image at 889 nm (MT3 filter) is projected as blue, and sees only the highest clouds (CH_4 absorption optical depth unity at 0.33 bars, according to CH_4 abundance derived by Tomasko and Doose (1984)). The image at 727 nm (MT2 filter) is projected as green, and sees high and intermediate clouds but not the lowest clouds (CH_4 absorption optical depth unity at 1.2 bars). The image at 750 nm (CB2 filter) is projected as red, is not limited by methane absorption and sees clouds at all levels. Each map is a mosaic from 27 images taken within ~5 h. The lower panel shows the storm ~11 h after the view in the upper panel. The latitudinal extent of the storm is ~10,000 km. West longitude and planetocentric latitude are labeled on the maps. The longitudes refer to the head of the storm on the first day, and are not accurate for the eastern end of the storm, whose images were taken 5 h later and moved with zonal wind. Further, the longitudes on the second day were shifted to the reference frame of the head, ensuring that the head lines up in the upper and lower maps. The images were taken by Cassini's narrow angle camera on February 26 2011 from a distance of $2.4 - 2.5 \times 10^6$ km, giving an image scale of ~15 km per pixel in CB2 images. The maps are made from the same data and use the same color scheme as Fig. 4 of Fischer et al. (2011a). The maps in this paper show the entire storm at higher spatial resolution than in Fischer et al. (2011a) (see Figs. 3–5), and include the lightning locations on the map. (For interpretation of the references to color in this figure legend, the reader is referred to the web version of this article.)

having absolute vorticity equal to zero, or $(\zeta + f) = 0$. Thus the fluid elements emerge from below with $\zeta = -f$. Most likely they acquire positive vorticity by mixing with their surroundings. Also, the head sheds anticyclones at a regular rate. This vortex shedding is different from that behind a blunt body, which sheds alternating vortices of opposite sign, forming a Karman vortex street in its wake. All of the large vortices to the east of the Saturn storm are anticyclones, so the wake is not a classic vortex street. And the head is not a blunt body; it is an active source of anticyclonic relative vorticity.

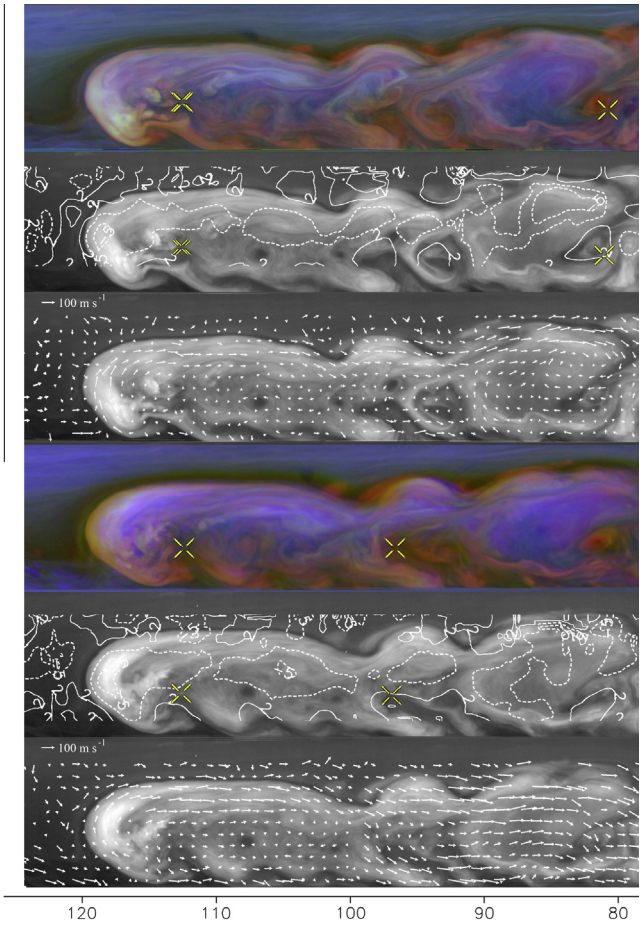

Fig. 3. High-resolution views of the storm on February 26 2011. Numbered from the top down, panels 1 and 4 are the western portions of the methane band mosaics shown in Fig. 2. Panels 2 and 5 are the corresponding contour maps of vorticity ζ overlain on the 455 nm (blue, or BL1) images. The contours of vorticity are 2, −2, and $-5\times10^{-5}\,s^{-1}$, respectively. Panels 3 and 6 are the corresponding velocity vectors δv overlain on the BL1 images. The white arrow halfway down on the left shows a velocity vector of $100\,m\,s^{-1}$. The uncertainty in velocities is $\pm5\,m\,s^{-1}$. Vorticity ζ and velocity δv are given in the reference frame of the head, which drifts to the west relative to the Voyager SKR frame at 2.79° per day (Sánchez-Lavega et al., 2011; Sayanagi et al., 2013). Each of the maps in Fig. 2 is a mosaic of 27 images in each filter taken every 10 min over a ~4.5 h period as the planet rotates beneath the spacecraft. Consecutive images overlap each other by a factor of ~2/3 and were used to make the velocity and vorticity maps. (For interpretation of the references to color in this figure legend, the reader is referred to the web version of this article.)

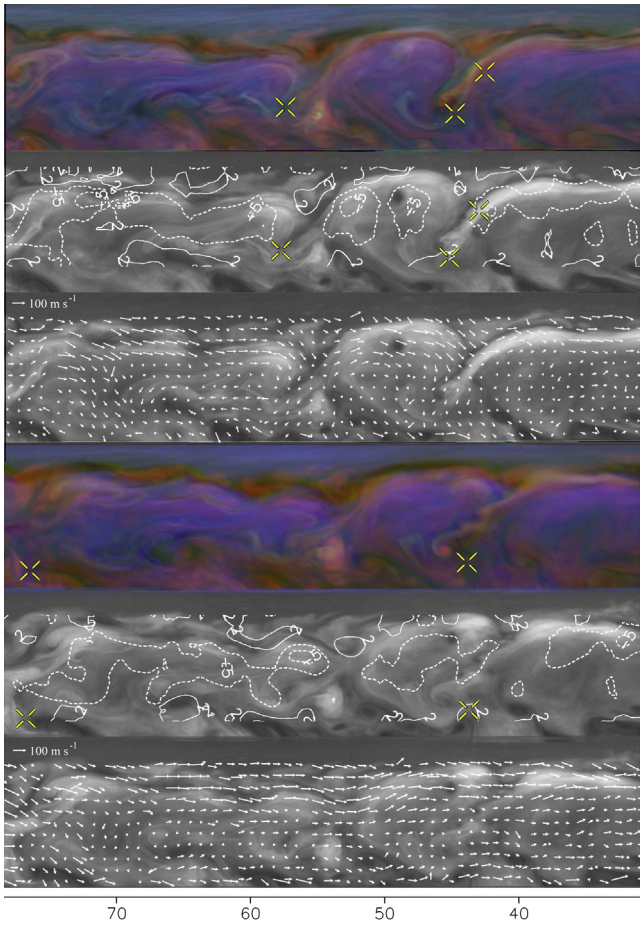

Fig. 4. Same as Fig. 3 but for the central portions of the methane-band mosaics shown in Fig. 2.

Here we speculate as to why the flash locations are near the large-scale diagonal southwest-directed disturbances in the storm, often next to the deep clouds with no clouds at higher atmospheric levels (red shades in false color in Figs. 2–5). One possibility is that the lightning is everywhere but it is covered up except in the red-shaded regions. This seems unlikely, especially for the blue-shaded regions, because they seem incapable of blocking light from below. These regions look blue because they are bright in the MT3 filter, which is a strong methane absorption band. The white and yellow regions are bright in the MT3 filter as well, but they are also bright in the MT2 and CB2 filters – the weak methane absorption band and the continuum where the gas is transparent, respectively. The interpretation is that the clouds visible in MT3 are a semi-transparent haze, because they allow one to see the light scattered from deeper clouds when those clouds are present. The blue-shaded regions do not have these deeper clouds and the white and yellow regions do. Thus the semi-transparent haze in the blue-shaded regions would not cover up the lightning if it were there. Thus the lightning is not uniformly distributed over the whole storm. It could be hidden beneath the white and yellow clouds, but it is not occurring beneath the haze in the blue shaded regions. It is possible that the deep clouds in the blue-shaded regions are black rather than absent, similar to infrared-dark clouds observed near the southern lightning storms (Baines et al., 2009). Such clouds could block the lightning optical emissions.

Although we have not proved it, let us assume that the lightning is only present in the diagonal features near the red-shaded regions. These are the only places where we observe lightning, and we are assuming that these are the only places where it is occurring. The diagonal features are located in the narrow gaps between the large anticyclones, where the winds are generally southward on the west side of the gap and northward on the east side. As a result, the gaps are cyclonic, and this can be seen in Figs. 3–5. Their red color in the methane band images signifies deep clouds with no high clouds overhead. In these two respects – cyclonic vorticity and absence of high clouds – the gaps are like the jovian belts, which also are the sites of lightning (Little et al., 1999; Porco et al., 2003). Although the occurrence of lightning in the jovian belts is not completely understood (Gierasch et al., 2000; Ingersoll et al., 2000), there may be some underlying process that generates lightning in cyclonic regions on both Jupiter and Saturn.

Deep winds at lightning levels can be roughly estimated from lightning. The two flashes marked as double yellow × sign in the first day's map in Figs. 2 and 3 were observed 20 min apart. The flashes are located at 110.8°/32.8° and 111.0°/33.1° longitude/latitude respectively (see Table A1 of the Appendix A). This means the lightning is flashing at the same location within the ±0.3°

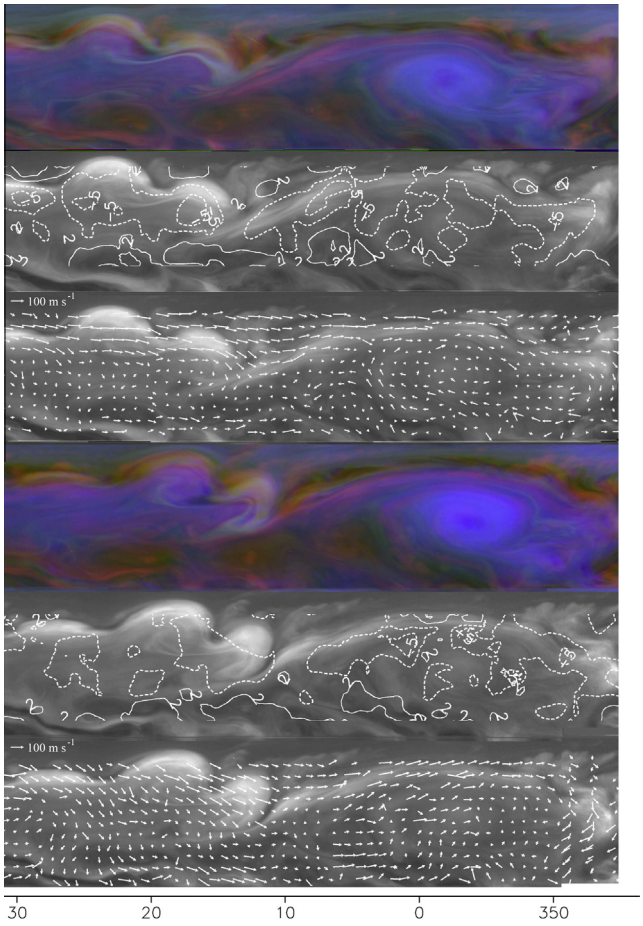

Fig. 5. Same as Fig. 3 but for the eastern portions of the methane-band mosaics shown in Fig. 2.

measurement uncertainty. Assuming the same location continues flashing till the next observation 11 h later, we can estimate its drift rate from that next observation. 11 h later a flash is observed at 112.8°/32.8°, which gives a drift rate of $2 \pm 0.3°/(11\ \mathrm{h}) = 40 \pm 6\ \mathrm{m\ s^{-1}}$ westward. Compared to the $26.9 \pm 0.8\ \mathrm{m\ s^{-1}}$ westward drift of the storm's head west edge reported by Sayanagi et al. (2013), this implies that the deep cloud moves west, approaching the head of the storm with relative speed $\delta v = 13 \pm 7\ \mathrm{m\ s^{-1}}$. At that speed, the lightning-producing cloud would reach the west edge of the storm in about 4 days. No lightning was observed past the edge by RPWS or the camera. This probably means that the deep lightning-producing clouds stop flashing or change their motion on their way to the west edge on the timescale of days. This is interesting because the head of the storm is the fastest westward moving feature on Saturn, and the lightning center exceeds that speed. It must be noted though that the wind calculation above is based on only 3 lightning flashes, and thus is uncertain. Also, it may not represent the deep winds in other parts of the storm.

Unlike the deep lightning-producing clouds, the observed cloud tops at the lightning location have a negligible speed of less than $5\ \mathrm{m\ s^{-1}}$ relative to the storm's head (see Fig. 3). The vertical wind shear between the cloud tops and lightning-producing level near the storm's head can also be estimated. The velocity of the deep clouds relative to the head is $\delta v = 13 \pm 7\ \mathrm{m\ s^{-1}}$ westward. Thus the wind difference between the upper clouds and the deep clouds (at the lightning level) is also about $\Delta v_z = 13 \pm 7\ \mathrm{m\ s^{-1}}$ increasing westward with depth. Similar wind difference can be also estimated for the southern storms of 2004. Dyudina et al. (2007) report that the spot repeatedly producing outbursts of bright clouds (probably a deep lightning storm) in 2004 drifts west at a rate 0.2° longitude per Earth's day. The bright clouds themselves drift west at a rate 0.8–0.9° per day. The difference is $\Delta v_z = 0.6$–$0.7°/\mathrm{day} \sim -6\ \mathrm{m\ s^{-1}}$. Note that in the south the winds decrease westward with depth. In addition to our small-number statistic estimate of the 2011 wind shear, there is the evidence of vertical wind shear at the western edge of the storm based on observed, possibly Kelvin–Helmholtz, wave structures (Ingersoll et al., 2013). The wind shears (13 and $-6\ \mathrm{m\ s^{-1}}$ in 2011 and 2004) define how fast the lightning-producing updrafts will be laterally moved away from lightning as they rise, as will be discussed in Section 7.

Fig. 6 shows one of the flashes, which can be seen in the exaggerated color image as a blue spot near the right edge of the one image (left panel), but not seen in the image 30 min later (right panel). As can be seen in false-color maps in Figs. 3 and 4, and in Fig. 6, at smaller scales of 100–300 km (0.1–0.3° latitude), the exact location of the flashes never coincides with bright clouds of similar size, though many such small-scale clouds can be seen in the storm. This probably means that these small clouds are not formed directly by strong convection and lightning.

Also, Figs. 2, 3, and 6 show that the lightning flashes in the 2011 storm are never within the high dense (white and yellow) clouds on the western edge of the storm's head. These clouds may be associated with other, undetectable, lightning, or may not be related to lightning (see discussion in Section 7). Lightning with no corresponding clouds is surprising because lightning in the South appears to be associated with high dense clouds, in 2004, 2006 (Dyudina et al., 2007), and in 2009 (Fig. 1).

3. Depth of the lightning

The lightning spot size indicates the depth of the lightning below the cloud tops. The ~200-km size of the blue spot in Fig. 6 is typical for all flashes detected in 2009 and 2011. Fig. 7 shows how brightness falls off with distance from the flash center for the two bright flashes: one seen on the night side in 2009, and the other seen on the day side in 2011 (flash from Fig. 6). The 2009 lightning was seen in the clear filter, and the 2011 lightning in blue. Brightness B in Fig. 7 is given per unit wavelength to compare images in different filters (see the definition of B in the Appendix A). Notice that the blue-filtered flash from 2011 has ~7 times the brightness of the 2009 flash, either due to stronger lightning, or due to an enhanced blue spectrum.

The half width at half maximum (HWHM) for flashes in Fig. 7, and for most of the other flashes, is about 100 km (see more plots in the Appendix A), indicating that all the flashes are at nearly the same depth. This confirms the conclusion of Dyudina et al. (2010) that the vertical distance between the lightning and the cloud tops is 125–250 km. With the new data we know that the cloud tops at lightning locations (red shades in Figs. 2–4) are deeper than expected by Dyudina et al. (2010). The tops are probably ammonia or NH_4SH clouds at depths exceeding 1.2 bars. This suggests lightning is even deeper, in the water clouds.

4. Simultaneous optical and radio lightning detections

The Cassini Radio and Plasma Wave Science (RPWS) instrument (Gurnett et al., 2004) detects radio waves emitted by lightning at frequencies from 16 MHz down to 1–2 MHz (Fischer et al., 2011b). The high-frequency limit is from the instrument; the low-frequency limit is the cut-off frequency of Saturn's ionosphere. The lightning signal consists of short radio bursts called Saturn Electrostatic Discharges (SEDs), which last for ~100 ms. It is interesting to compare the radio signal with the optical signal, both

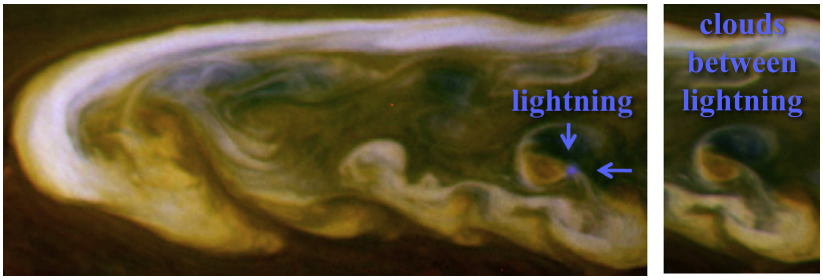

Fig. 6. Approximately true color image of the storm showing a lightning flash in blue. For each panel, the images in near infrared filter CB2, green, and blue were taken within 1 min, and were combined as red, green, and blue respectively. Images in blue were stretched in contrast to bring up the lightning – a diffuse spot in the image. Similar stretching in other filters does not reveal lightning. The images were map-projected. The image in the left panel was taken on March 6, 2011 at 18 h. 36 m. 51 s (see flash details in Table A1 of the Appendix A). The image in the right panel was taken 30 min later. (For interpretation of the references to color in this figure legend, the reader is referred to the web version of this article.)

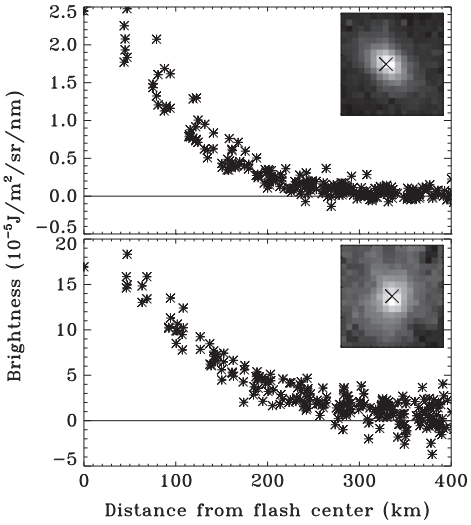

Fig. 7. Brightness distribution in lightning flashes on November 30, 2009 at 20 h 38 m 18 s (upper panel) and on March 6, 2011 at 18 h 36 m 51 s (lower panel) (see details in Table A1 of the Appendix A). Brightness B is plotted versus distance from the flash center measured along Saturn's surface. The background brightness was subtracted from the images, which resulted in a mixture of positive and negative brightness values. The insets in the right top corner of each plot show the unprojected image of the corresponding flash where the flashes are foreshortened due to slant viewing. The $\times$ symbol indicates the assumed flash center.

with respect to timing and energy of individual flashes and with respect to the average power emitted by the storm over a period of days.

The two sets of nightside observations in 2009 had exposure durations of 15–180 s with tens of seconds between the images. Each set spanned tens of minutes. The dayside observations in 2011 had exposure durations of a fraction of a second with tens of minutes between the images. These observations spanned tens of hours. The timing details can be found in Table A1 of the Appendix A. For all of the detections the RPWS instrument was on and was detecting SEDs in radio frequencies.

Fig. 8 compares optical lightning detections with simultaneous SEDs. Lightning spots in the images are probably single instantaneous flashes rather than repeated flashes accumulated at the same spot (see Section 2). Accordingly, we can calculate the energies of the instantaneous flashes. Cassini camera registers only part of the visible light that falls within the corresponding filter (clear or blue). Our energy estimates include only the light coming through the filter bandpass.

We calculate the optical energy of the several-pixel-wide lightning spots E_o. Following Little et al. (1999) and Dyudina et al. (2004) we treat each flash as a patch of light on a Lambertian surface, so that both upward and downward fluxes were assumed to be π times the intensity. Intensity is power per unit area per solid angle, which is $B \cdot \Delta\lambda/t_{exp}$, where t_{exp} is exposure time and B is spectral brightness in J m^{-2} sr^{-1} nm^{-1} (see Section 3). The corresponding total power would be 2π times the intensity times the area of the emitting patch. Multiplication by t_{exp} converts power to energy E_o, and then t_{exp} cancels out.

$$E_o = \sum_{pix} \frac{2\pi B \cdot \Delta\lambda \cdot (PixelArea)}{cos(e)}, \quad (1)$$

where B is the brightness for each pixel minus background, $\Delta\lambda$ is the effective filter width (800 and 100 nm for clear and blue filters), pixel area is measured in the image plane and equals the square of the pixel size, e is the emission angle measured from the local vertical, and the sum is taken over all lightning spot pixels.

The strongest flashes in the 2009 storm are detected during the 120-s exposures (higher energies in the upper panel of Fig. 8). Weaker flashes are detected in short 15-s exposures. Counting only 15-s exposures, the flash rate is about 1–2 flashes per minute, as calculated in Section 2. During longer exposures the background noise level is higher, which makes lightning harder to identify. As a result, in four 120-s images 7 flashes can be identified, giving a rate of 0.9 flashes per minute, slightly less than the 1–2 flashes per minute derived from the short exposures. For the further reference we will quote the flash rate of 1 per minute for this storm.

The SED data taken at the same time as optical data are shown in the lower panel of Fig. 8. The RPWS instrument scans in radio frequency and is capable of detecting SEDs only for 1/3 of each of the ~16-s scan periods, so statistically only 1/3 of the SEDs can be detected. 2/3 of the time are "blind" periods during which RPWS scans frequencies below the ionospheric cutoff frequency (~2 MHz) or is simply waiting to start the next scan. These blind periods are shaded gray in the SED plot.

The energy of the SEDs is given in units of spectral source power W/Hz, or simply SED power. This is a convenient unit for a source that emits at a constant rate (power), but it is less convenient for lightning, whose duration is short and whose integrated emission (energy) is what matters. To convert to spectral energy J/Hz, one must multiply the SED power by the 35.2 ms integration time for each frequency channel. The RPWS sweeps through ~28 frequency channels per second, often capturing a single lightning flash at several different frequencies in succession. Energy is calculated from the incident radio flux assuming isotropic radiation from the source (Fischer et al., 2006a). To get the total spectral energy from a single flash, one must add the contributions of each channel. At flash rates greater than about 10 per second the flashes overlap. Then it becomes difficult to resolve individual flashes. To convert spectral energy to total energy, one must multiply by the total

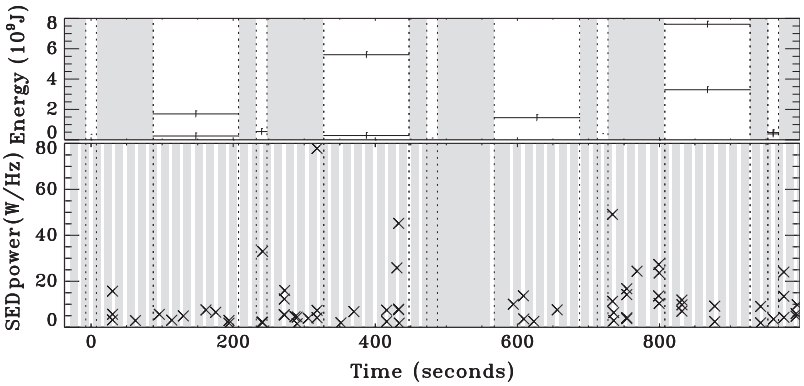

Fig. 8. Energy of individual optical flashes versus time, counting from the middle time of the first image in Fig. 1 (November 30, 2009, at 20 h 31 m 43.5 s), in upper panel, compared to the SED radio spectral source power (lower panel). We call these measurements "SEDs" and not "SED pixels" as in previous papers (see the Appendix A). The uncertainty in optical flash energy (vertical error bars in the upper panel) is due to the pixel noise in the images. The image exposure durations, which define uncertainty in time for each flash, are shown as horizontal error bars. The start and end of each exposure is also shown by the vertical dotted line in order to be compared with SED timing. During the times between the end of one exposure and the beginning of the next exposure the camera was not observing. These no-data times are shaded gray. The vertical dotted lines in the lower panel are start/end times of the camera continued from the upper panel. The "blind" times when RPWS cannot detect SEDs are shaded gray.

frequency range of the SED emissions, and that is highly uncertain. It could be any value from 100 MHz to 100 GHz (Lewis, 1982; Farrell et al., 2007).

Comparison of SEDs with visible flashes in Fig. 8 is complicated because less than 1/3 of the SEDs are detected due to multiple "blind times" during the long image exposures. Also the flash timing is uncertain: they could have occurred at any time during the exposure. No clear correlation between SED and visible flashes is seen during the 120-s exposures in Fig. 8. However, there is clear correlation between flashes and SEDs during the 15-s exposures, namely, out of five short exposures, two show both visible flashes (at 240 and 1000 s) and SEDs, and the other three show neither flashes nor SEDs.

The 2011 images were taken with very short exposures of a fraction of a second. As a result, only five out of ten 2011 optical flashes had simultaneous SEDs, others fell into RPWS "blind" times. These five flashes are shown in Fig. 9. Unlike 2009 data, no blind times occurred during flash exposures in Fig. 9. Hence, all of the SEDs produced by the storm during the flash exposures are detected. However, the 2011 SED/flash comparison is also tricky because the camera is not observing the whole storm as it does in 2009. In 2011 only ~1/4 of the lightning-active region between 40° and 115° longitude is observed at any given time. As a result, a large fraction of lightning which produced SEDs in Fig. 9 was flashing outside the camera's field of view, i.e., was optically undetectable.

To derive the optical flash rates of February 26 2011, we needed to account for such incomplete coverage by the camera. Each location of the storm was covered by about 5 blue-filtered images. The corresponding duration of the survey is 5 times the exposure (5×0.38 s = 1.9 s, see details in Section 2 of the Appendix A). In other words, the whole storm was observed for 1.9 s, though not simultaneously. Accordingly, the 10 flashes detected on February 26 2011, give a rate of ~5 flashes per second for the whole storm.

A few very strong multiple-SED narrow vertical peaks can be seen in Fig. 9. Each of them probably belongs to a single very strong lightning strike. In the three upper panels (February 26 data), none of these peaks coincide with optical flashes. These flashes are relatively faint ($2–4 \times 10^9$ J). The SED powers during these flashes (between the dotted lines) are less than 20 W/Hz: some of these SEDs are probably produced by lightning elsewhere in the storm.

Luckily, the large flash on March 6 (blue flash in Fig. 6) was observed during SED-sensitive rather than SED-blind time (lower panel of Fig. 9). There is a prominent multiple-SED peak which was probably produced by that flash. We cannot exclude that these SEDs come from elsewhere in the storm, but it seems unlikely. Indeed the optical flash is unusually bright ($\sim 8 \times 10^9$ J), and the SED peak is unusually strong. The perfect temporal correlation gives us additional confidence that both optical and the SED signals come from the same lightning.

Table 1 summarizes SED and optical properties of each flash in Fig. 9. The lowest SED activity is produced by the flash at February 26 16:34:14. It corresponds to 3 SEDs. The SED rate is close to the average non-SED-peak rate of 4–10 SEDs per Section (2–4 SEDs per the 0.38 s exposure). Accordingly, the low-rate SEDs for this flash are probably the least contaminated by SEDs happening in the storm outside of the camera's field of view. Given such contamination it is surprising that the optical flash energies are proportional to the SED numbers to high accuracy (line 3 in Table 1). It is especially puzzling because the SED powers are different for different flashes (see Fig. 9). The total SED powers are not proportional to the optical flash energies (in Table 1, the ratios Σ(SED powers)/E_o range from ~13 to ~200). This may be due to nonlinearity of SED powers with optical flash energy, or due to some unknown observational bias. Of course with just one flash associated with the strong SED peak, we cannot exclude that these SEDs came from unobserved parts of the storm, and then the Σ(SED powers)/E_o ratio for that flash is irrelevant. We consider the SED/optical relation from the February 26, 16:34:14 the most confident of our estimates. It gives $\Sigma(\text{SED powers})/E_o \sim 13 \times 10^{-9}$ W Hz^{-1} J^{-1}.

5. Energies and flash rates

5.1. Optical and radio powers of the storms

We estimate the optical P_o and radio P_r powers of the three lightning storms on Saturn. Table 2 compares the results with lightning storms on Jupiter. To get the 2009 storm power we add up optical energies E_o of all detected lightning and divide by the total survey time. To get the 2011 storm power we add up optical energies E_o of all detected lightning and divide by the typical survey time of 1.9 s (see Section 4 and the Appendix A). Energies of 2011 flashes, seen through the 100-nm-wide blue filter, are likely underestimated by a factor of a few compared to 2009 energies, seen through the 800-nm-wide clear filter. The exact energy conversion between the filters is uncertain because of the non-flat filter shape (Porco et al., 2004) and because of the unknown lightning spectrum.

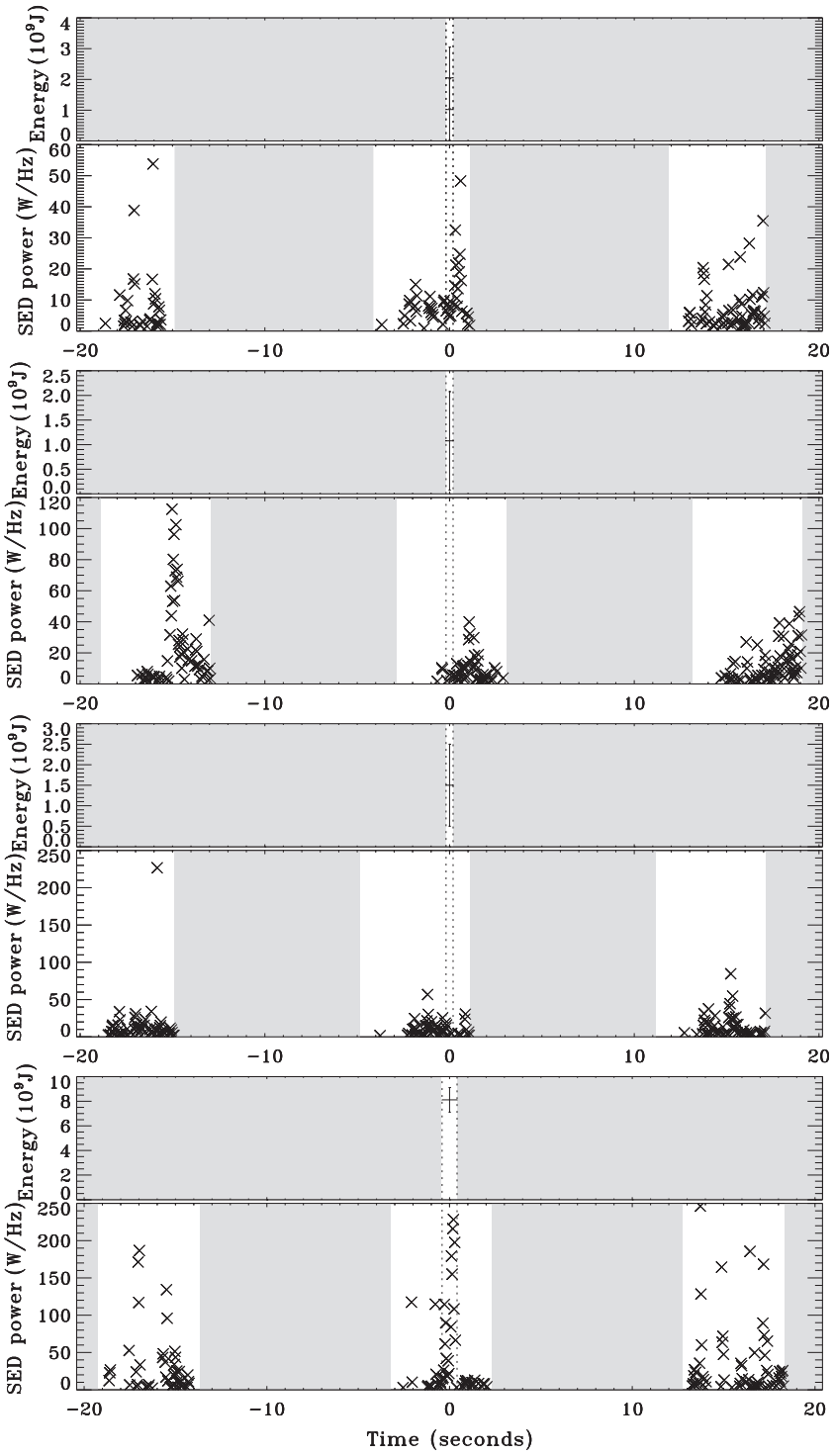

Fig. 9. Energies of the dayside flashes and their timing counting from the middle of each flash exposure, compared to the SED spectral source power. The data are plotted the same way as in Fig. 8. Panels correspond to flashes at times: 2011-057T04:45:45 (two flashes detected in one image), 2011-057T16:34:14, 2011-057T17:03:20, and 2011-065T18:36:51 top to bottom, see details and error bar discussion related to Table A1 of the Appendix A.

The average radio spectral powers of the storms are given in Table 2. We assume that they are radiated over a frequency range of 10 GHz. Radio emissions of terrestrial lightning have been measured up to this frequency, and the spectral amplitude falls off at least as fast as inverse of the frequency above 10 kHz (Lewis, 1982). By contrast, at Saturn the 1–16 MHz SED spectrum is relatively flat (Fischer et al., 2006b). We do not know the spectral behavior of SEDs over the full radio range, and different models can lead to a variation in total radiated energies over several orders of magnitude (Farrell et al., 2007). The storms' radio powers P_r listed in Table 2 assume flat-spectrum radiation across the 10 GHz, and are therefore uncertain.

Both optical and radio powers of the 2010–2011 storm are much higher than the powers of the 2009 storms, but only because of higher flash rates. The optical energies and SED spectral powers of individual flashes in Table 2 are comparable in 2009 and 2011.

Table 1
Number and energies of SEDs in 2011 corresponding to the optical lightning shown in Fig. 9. The time is given in the format (hour:minute:second).

Date	February 26	February 26	February 26	March 6
Time	04:45:45	16:34:14	17:03:20	18:36:51
E_o (10^9 J)	1.0 and 2.1	1.1	1.5	8.3
Number of SEDs	7	3	4	20
ΣE_o/Number of SEDs (10^9 J)	0.45	0.34	0.37	0.42
Σ(SED powers) (W/Hz)	47.3	13.8	27.6	1701.4
Σ(SED powers)/ΣE_o (10^{-9} W Hz^{-1} J^{-1})	∼15	∼13	∼18	∼200

5.2. Scaling between optical and radio signals from lightning

Optical data provide the most accurate estimates of Saturn lightning energies, but there are only few optical observations. They cannot give good statistics on highly variable lightning storms. SEDs provide excellent statistics and temporal coverage of the storms,but it is difficult to connect individual optical lightning flashes to specific SED measurements. Hence it is essential to know the scaling between the observable SED spectral source powers and optical energies (SED power)/E_o to understand long-term energetics of the storms.

The radio to optical power ratio P_r/P_o in Table 2 ranges between 7 and 27. This time-averaged ratio gives a very rough estimate of the ratio E_r/E_o for individual flashes because the small number of optical detections may not represent the important high-energy end of the energy distribution contributing to P_o. Also, the values of P_r/P_o may be biased due to different sensitivity levels of the camera and RPWS (see sensitivity discussion in Section 7). However P_r/P_o of 7 to 27 in Table 2 suggests that E_r and E_o may also be of the similar order of magnitude, as it is on Earth (Uman, 1987). On Saturn ∼0.1% of the total lightning energy is expected to go to the optical energy (Borucki and McKay, 1987), similar to 0.1-few % of the total lightning energy going to the radio on Earth (Volland, 1982).

To derive a less biased scaling (SED power)/E_o we compare energy versus flash rate distributions in radio and optical observations. Fig. 10 shows such cumulative energy distributions for three different dates. The ordinate of the optical points in Fig. 10 indicates the number of optical flashes that are brighter than a particular energy level (abscissa), detected per second of the survey time. The total flash rate including all detected flashes regardless of their energies is the maximum ordinate value for each data set.

The lower limit for the flash rate on the ordinate for each data set corresponds to 1 count per survey time, and indicates that lightning flashing at lower rates cannot be detected with similar-length surveys. With longer surveys, it is likely that brighter but rare flashes could also be detected, i.e., the distributions would continue towards less frequent lightning with higher energies. The lowest optical energy for each date is defined by detection limit of the images, and is different for each data set. Because flashes at lower energies are detected in larger numbers, we expect even more lightning below the detection limit.

Similarly to optical data, the ordinate of the SEDs in Fig. 10 indicates the number of SEDs stronger than a particular SED power, detected per second of SED survey time. The SED powers are given for single 35-ms SED measurements, which do not always correspond one to lightning flashes. One lightning flash usually lasts longer than 35 ms and spans on average 2 consecutive SED measurements (Fig. 6 of Fischer et al. (2007), the 2011 SEDs show similar distribution). Additionally, in the 2011 storm, the lightning rate is so high that signals from several lightning flashes often overlap, with two or more lightning contributing to one SED measurement. Because of such uncertainties, the SED and optical counts cannot be easily related, though we expect between 1 and 20 SEDs per optical flash and a constant optical energy per SED (see Section 4).

We assume a single SED per optical flash in 2011 because it is the simplest of possible relations, and because the shapes of the 2011 SED and optical curves fit well under this assumption. Then we fit the 2011 optical and SED curves by scaling the energies. The corresponding ratio is (SED power)/$E_o = 8 \times 10^{-9}$ W Hz^{-1} J^{-1}. It is close to the ratio derived for February 26, 16:34:14 flash in Section 4. In that case three SEDs of powers less than 8×10^{-9} W Hz^{-1} J^{-1} added up to give Σ(SED powers)/$E_o \sim 13 \times 10^{-9}$ W Hz^{-1} J^{-1} per multiple-SED flash.

The August 2009 flashes were imaged during the 12 min of unusually quiet lightning activity, when only 4 SEDs were detected (blue × symbols in Fig. 10). This is about 5 times less than the one-hour-averaged rate (dotted line). The SED rate during these 12 min is about the same as the optical flash rate, giving one SED per one optical flash, as reported by Dyudina et al. (2010). The same (SED power)/E_o ratio that fits 2011 data gives a good fit between August 2009 optical flashes and SEDs (blue triangles fit blue × symbols).

The November 2009 SED rates (dashed line) are ∼10 times higher than the optical flash rates (green diamonds) for low energy flashes. The two flashes with the highest optical energies fit the SED rates. The November 2009 optical data set is based on images with two different exposure times (see Fig. 1). That may have introduced an underestimate of optical counts for low-energy flashes, which are less detectable with long-exposure images. Radio detection efficiency should not create a bias between different dates because it is similar in all three data sets (see Appendix A).

The ratio (SED power)/$E_o = 8 \times 10^{-9}$ W Hz^{-1} J^{-1}, which assumes one optical flash per one SED (and which was used to scale Fig. 10)

Table 2
Optical and radio characteristics of lightning on Jupiter and Saturn. Jupiter data are the brightest flash and power of the 1997 "scanned" Storm 10 observed by Galileo (Little et al., 1999), and similar results from 2007 New Horizons observations by Baines et al. (2007). Single SED average spectral power was calculated as the average of all SEDs detected within 5–7 h. Storm's radio spectral power is an average over detections and non-detections and thus is a smaller number since SEDs are not radiated permanently. It is calculated by multiplying the average SED spectral power by the integration time of 35 ms and by the SED rate. No SEDs were detected on Jupiter.

	Jupiter	Saturn night August 2009	Saturn night November 2009	Saturn day February 26 2011
Filter	Clear	Clear	Clear	Blue
Brightest flash energy E_o (J)	1.57×10^{10}	1.6×10^9	7.6×10^9	4.4×10^9
Optical survey time	149.4 s	720 s	555 s	1.9 s
Optical flash rate	0.3 per second	1 per minute	1 per minute	5 per second
Optical power of single storm P_o (W)	0.674×10^9	7.5×10^6	3.9×10^7	1.2×10^{10}
SED rate		4 per minute	7.7 per minute	10 per second
Single SED average spectral power (W/Hz)		8.7	7.4	22.4
Storm's radio spectral power (W/Hz)		0.02	0.034	8.2
Storm's radio power P_r (W)		2×10^8	3.4×10^8	8×10^{10}
Radio to optical ratio P_r/P_o (W per W)		27	9	7

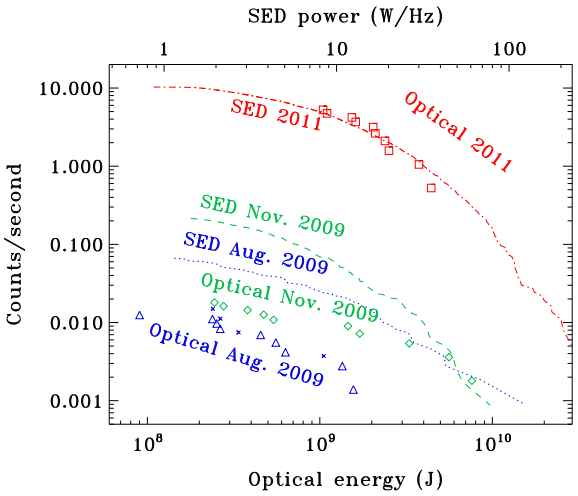

Fig. 10. Cumulative distribution for the optical energy of optical flashes and for the spectral powers of individual 35 ms-long SEDs. Optical energy is shown by open triangles, open diamonds and open squares for August 2009, November 2009, and February 26, 2011, respectively. Colors indicate the date of observation for both optical and radio data. The ordinate is the rate of the optical flashes that have energies shown on the abscissa or larger energies. For SEDs the ordinate is the rate of the SEDs that have spectral powers shown on the abscissa or larger powers. These rates are derived by sorting the total number of detections n in each survey by decreasing energies, assigning each detection a number (n to the faintest, $n-1$ to the next faintest, … 1 to the brightest), and then dividing the numbers by the corresponding survey time. Dotted, dashed, and dot-dashed lines show SEDs for August 2009, November 2009, and February 16, 2011, collected over 1084, 1146, and 366 s, respectively. The corresponding optical survey times are 720, 555, and 1.9 s. The SED surveys were done within an hour of the optical flashes and exclude the RPWS "blind" times. The blue × symbols indicate SEDs detected during the August 2009 optical survey, i. e., between the beginning of the first image and the end of the last image. The scaling between the optical energy and SED spectral power (in W/Hz) is chosen to fit 2011 SEDs to the optical curves. (For interpretation of the references to color in this figure legend, the reader is referred to the web version of this article.)

fits the Aug 2009 and 2011 storms, and probably also the November 2009 storm. We convert this ratio to E_r/E_o by multiplying SED spectral powers by 35 ms and 10 GHz, similarly to calculations for Table 2. This gives $E_r/E_o \sim 3$. This ratio is physically equivalent to P_r/P_o from Table 2, which is 27, 9, and 7 for the three storms. For August 2009, $P_r/P_o = 27$ is not representative because it relates the 1-h average SEDs to unusually quiet 12 min of optical observations. The November 2009 and February 2011 ratios of 9 and 7 are comparable to 3, but the ratio of 3 is less biased. Again $E_r/E_o \sim 3$ tells us that, as on the Earth, the optical energy radiated by Saturn lightning is probably of a similar order of magnitude as the radio energy.

5.3. Convective power of the 2011 storm derived from lightning optical power

On Earth, a large fraction of the energy transported from the surface to space is carried by precipitation in thunderstorms forming mesoscale convective systems (Houze, 1993). It is interesting to estimate the role of thunderstorms in the global energy balance on Saturn. We do that using the time-averaged optical lightning storm power P_o. The 2011 storm produces $P_o \approx 10^{10}$ W (see Table 2). The optical efficiency (converting total lightning bolts' energy to light) on Saturn should be close to the laboratory-measured efficiency of laser-induced plasma (LIP) in an 87% H_2, 13% He gas mixture, which represents lightning on Jupiter (Borucki and McKay, 1987). They report the efficiency of $E_o/E_t = 1 \times 10^{-3} \pm 32\%$, where E_t is the total energy released by the lightning discharge (which includes thunder, heat, light, and electromagnetic waves). Accordingly, the total power released by lightning flashes in the 2011 giant storm flashes would be $P_t = E_t/E_o \times P_o \approx 10^3 \times P_o \approx 10^{13}$ W. On the Earth, the global lightning flash rate is 44 ± 5 flashes/s (Oliver, 2005). The average energy is $E_t \approx 3 \times 10^9$ J (Borucki et al., 1982; Turman, 1978). This gives the total terrestrial lightning flash power of $P_t \approx 1.3 \times 10^{11}$ W. The 2009 lightning storms in Saturn's southern hemisphere produce about 10 times less lightning flash power than all terrestrial thunderstorms combined ($P_t \approx 10^3 \times P_o \sim 10^{10}$ W, see P_o in Table 2). Saturn's 2010–2011 giant storm produces about 100 times more lightning flash power than all terrestrial thunderstorms. With Saturn's area of ~83 times the Earth's area, terrestrial powers per unit area is almost the same as Saturn's during the 2011 storm. At quieter times with smaller storms or no storms, Saturn produces much less lightning power per unit area than the Earth.

To estimate the moist convective updraft energy flux P_c in Saturn's giant storm, we need to convert lightning flash power P_t to that flux. The energetic efficiency of convective updrafts in producing lightning flashes P_t/P_c is not known for Saturn. We use the terrestrial value as a rough estimate. Piepgrass et al. (1982) finds $\sim 2 \times 10^4$ m^3 of rainfall per flash in Florida's storms. This releases $E_c \sim 4 \times 10^{13}$ J of condensation latent heat. As discussed above, the typical terrestrial flash energy of $E_t = 3 \times 10^9$ J. This gives the efficiency $P_t/P_c \approx E_t/E_c \sim 10^{-4}$. Similarly, (Borucki et al., 1982; Lewis, 1980) estimate the terrestrial ratio of energy dissipated by lightning to convective energy flux to be 10^{-4}.

Applying this to Saturn's 2011 storm, lightning flash power $P_t \approx 10^{13}$ W translates into convective energy flux of $P_c \sim 10^{17}$ W. Given the high uncertainty in lightning-producing efficiency of storms for Saturn, we expect our calculation to be uncertain by at least an order of magnitude. Note that the 2011 storm's optical power was likely underestimated by a factor of few due to its blue-only wavelength range. Additionally, our optical powers are underestimated for all storms because cloud attenuation is assumed to be zero. In reality, clouds probably dimmed the flashes at least by another factor of few (Dyudina et al., 2002). Accordingly, our visible-light-based storm power value of $P_c \sim 10^{17}$ W likely underestimates the storm's convective energy flux.

This power is close to the 2×10^{17} W of total power emitted to space in the infrared by the whole surface of Saturn. Another order of magnitude estimate of the storm's contribution to Saturn's emitted power was based on the cloud's volume and corresponding latent heat of condensed water (Fischer et al., 2011a). According to that estimate, the 2010–2011 storm produces energy comparable to the total internal heat radiated by the planet in a year, assuming the internal power is (0.78/1.78) times the total radiated power (Hanel et al., 1983). The estimate by Fischer et al. (2011a) involves many unknowns such as water mixing ratio, convective updraft heights, and vertical thickness of the storm clouds. However, both estimates consistently indicate that the storm's power is comparable to Saturn's total radiated power. With such a large power output, it is clear that the 2010–2011 storm, and probably other Great White Spots play a key role in convective cooling of Saturn's interior.

6. Spectral data

Although only blue images showed day side lightning, this is due to an observational bias and does not indicate the blue color of lightning, as is explained below.

Cassini observations were planned years in advance, with no capability to repoint the camera to the giant storm's location. As a result, only two sets of images of the giant storm taken by the Narrow Angle Camera (NAC) had high enough spatial resolution to detect 200-km-scale lightning spots. Both of them, among other filters, used blue filter (BL1) and detected lightning with this filter

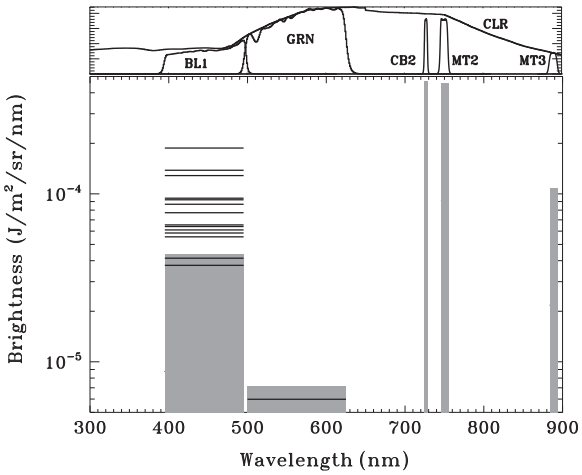

Fig. 11. Lightning detection limits of the images at different wavelengths. Upper panel: spectral shape of Cassini narrow angle camera's filters BL1, GRN, CB2, MT2, and MT3 convolved with optics transmission and detector sensitivity (see details in Porco et al. (2004)). Lower panel: Brightness B of detected lightning (solid horizontal lines), and $5 \times \sigma$ noise levels in the 2011 storm images taken with different filters (grayscale bars). The length of the solid lines and the width of the bars shows the width of the corresponding filter. The height of the grayscale bars represents the detection limit for each filter.

(see Table A1 of the Appendix A). The first set of images on February 26 2011 detected the most lightning because the same areas in the storm were covered by multiple images (2–3 times within 20 min). Multiple coverage close in time is essential for dayside detection (see our lightning detection technique in the Appendix A).

In addition to BL1 images with exposure time of 0.38 s, the February 26 2011 observation was also taken with CB2, MT2, and MT3 filters. These filters are narrow-band in wavelength, which required longer exposures of 3.2, 18 and 22 s, respectively. During longer exposures background pixel noise accumulates in the images. In contrast, the instantaneous lightning flashes contribute the same signal to the image regardless of the exposure. With the same signal and larger noise the longer exposure images are less sensitive to lightning.

To predict lightning detectability with filters other than BL1, we assumed that lightning would be detected at similar signal to noise levels as in BL1. For lightning flashes in BL1, we measured signal to noise ratio, i.e., for each flash we compared the brightest pixel above the background with standard deviation of the pixel noise σ in the BL1 images. For the faintest flashes the brightest pixel was about $5 \times \sigma$. Because we expect even fainter flashes to occur in this storm (see Section 5), our detection is limited by the noise level, and not by the absence of faint lightning. To define detection limit in other filters used in 2011 observations we also measured the pixel noise in these images. We assumed that the detection limit in other filters is also $5 \times \sigma$.

Fig. 11 shows the lightning detections and the $5 \times \sigma$ noise levels for the February 26 2011 observations as seen with different filters. Note the logarithmic scale of the brightness. For the BL1 filter, the faintest detections (black horizontal lines) are close to the $5 \times \sigma$ noise levels (grayscale bar). For CB2, MT2, and MT3 the $5 \times \sigma$ detection limits are considerably higher. If lightning had a flat spectrum, we would expect the flashes appear in CB2, MT2 and MT3 at the same level of B as in BL1. Also, the flashes would appear in similar or larger numbers as in BL1, because the longer exposures provide longer survey time. Apparently, none of the flashes detected in BL1 would be detected in CB2 and MT2 because of the higher noise. It is possible that the brightest flashes seen in BL1 would still be detectable in MT3, if the lightning spectrum were flat. However, MT3 covers a strong methane absorption line of Saturn's atmosphere, which should substantially dim the lightning signal at these wavelength, so we do not expect to see detections in MT3.

An interesting and highly controversial lightning detection is shown in the green filter (GRN) in Fig. 11. The green filter data are from the March 6, 2011 data set. This data set had much smaller spatial coverage than the February 26 data set. Less than 1/4 of the storm area was repeatedly covered by pairs of images on March 6. It made lightning detection much less probable, and only one flash was detected in BL1. On March 6 the storm was observed in three filters: BL1 with exposure 0.82 s, CB2 with exposure 1.5 s, and green (GRN) with exposure 0.04 s. The short exposure in the green filter made the images much more sensitive to the fainter lightning (grayscale bar in Fig. 11 shows much lower detection limit for GRN compared to BL1). At the same time the chance for the lightning to flash during the 20 times shorter exposure is 20 times lower in GRN than in BL1. Flashes bright enough to be seen in BL1 occur at a rate of about 5 per second (see Table 2) for the whole storm, more than half of these flashes in the most active area in the storm's head. The chances to see one of the storm's head flashes with the 0.04-s exposure of the GRN images are of the order of 1/10. However fainter and more frequent flashes not detectable in BL1 may be detected in GRN images.

The only detection in GRN is highly controversial because the possible flash falls right at the edge of the image, and may be confused with some unknown camera's edge effect. The reason to believe that the flash in GRN may be real is that it appears in the most active area in the storm's head.

Unfortunately, with all the analysis presented here, the question of saturnian lightning spectrum remains open. The CB2, MT2, and MT3 images are too noisy to detect lightning, and the possible lightning in GRN cannot be compared with BL1 lightning because they sample different parts of the energy/(flash rate) distribution.

7. Discussion

7.1. Lightning in cloudless regions and dense clouds

The absence of lightning detection in the dense white clouds at the west edge of 2011 storm (Figs. 2, 3, and 6) is surprising. The presence of such white clouds on Saturn typically indicates thunderstorms. The flashes in the 2009 storm in Fig. 1 are usually at the edge, and not in the middle of the bright cloud. One explanation of such off-cloud location is that the bright clouds are optically thick and block the light from lightning. Accordingly, lightning is flashing underneath the clouds, but it is not observable. This explanation seems sufficient for the 2009 lightning in Fig. 1, where flashes are seen directly at the edge of the cloud. It is easy to expect that the lightning is flashing under the cloud but can be seen only at the edge where the cloud is thinner. In the 2010–2011 storm (Figs. 2 and 6), none of the flashes are observed inside or at the edge of the white clouds. Instead, all the observed flashes are far from these clouds, and the cloud-blocking explanation seems less likely. Also, in white water or ammonia clouds the diffuse scattering should not be very effective in blocking the light from lightning. For terrestrial thunderstorms observed from a high-altitude airplane by Christian and Goodman (1987), the total light emitted to space by lightning-illuminated clouds is similar to the light from cloud-to-ground lightning seen underneath the clouds. Similar low cloud blocking was also modeled for terrestrial clouds by Thomason and Krider (1982). Modeling of Jupiter's cloud scattering by Dyudina et al. (2002) shows that it reduces light from lightning by a factor of 10 at cloud optical depths of ~30. Also, lowering

Table A1
Characteristics of optical lightning flashes detected on Saturn. See description in the text.

Image name	Date (yr)-(day)T(time)	Filter	Lon (deg)	Lat (deg)	km/pix	t_{exp} (s)	e (deg)	E_o (10^9 J)	B (10^{-6} J/(m^2 sr nm))
N1629172541_5	2009-229T03:11:59.185	CL1	10.9	−36.2	26	180.	31	0.09	1.89
N1629172741_5	2009-229T03:15:19.183	CL1	11.0	−36.4	26	180.	31	1.56	4.91
N1629172741_5	2009-229T03:15:19.183	CL1	10.4	−36.3	26	180.	31	0.25	0.86
N1629172941_5	2009-229T03:18:39.182	CL1	11.2	−36.2	26	180.	31	0.26	1.31
N1629172941_5	2009-229T03:18:39.182	CL1	10.5	−36.2	26	180.	31	0.63	1.65
N1629172941_5	2009-229T03:18:39.182	CL1	10.0	−36.3	26	180.	32	0.55	1.80
N1629173141_5	2009-229T03:21:59.181	CL1	11.3	−36.3	26	180.	32	0.23	1.10
N1629173141_5	2009-229T03:21:59.181	CL1	10.6	−36.3	26	180.	32	1.35	3.26
N1629173141_5	2009-229T03:21:59.181	CL1	10.0	−36.2	26	180.	32	0.45	1.76
Σ over storm	2009-229	CL1				720.	32	5.4	
N1638307115_1	2009-334T20:34:18.509	CL1	47.3	−35.8	30	120.	24	0.24	4.82
N1638307115_1	2009-334T20:34:18.509	CL1	46.6	−36.1	30	120.	25	1.70	4.36
N1638307155_1	2009-334T20:35:51.012	CL1	46.9	−36.0	30	15.	25	0.53	2.04
N1638307355_1	2009-334T20:38:18.511	CL1	46.3	−36.4	30	120.	25	5.60	24.76
N1638307355_1	2009-334T20:38:18.511	CL1	47.9	−36.1	30	120.	25	0.27	5.51
N1638307595_1	2009-334T20:42:18.513	CL1	47.4	−35.9	30	120.	25	1.45	5.32
N1638307835_1	2009-334T20:46:18.523	CL1	46.8	−36.0	30	120.	26	3.29	8.59
N1638307835_1	2009-334T20:46:18.523	CL1	46.2	−36.5	30	120.	27	7.61	31.71
N1638307875_1	2009-334T20:47:51.027	CL1	46.9	−36.0	30	15.	27	0.47	2.98
N1638307875_1	2009-334T20:47:51.027	CL1	47.2	−35.7	30	15.	26	0.38	1.52
Σ over storm	2009-334	CL1				555.		22	
N1677388449_1	2011-057T04:26:21.134	BL1	42.3	35.0	28	0.38	24	2.51	60.98
N1677389613_1	2011-057T04:45:45.126	BL1	44.7	31.9	28	0.38	20	1.04	37.54
N1677389613_1	2011-057T04:45:45.126	BL1	55.5	33.0	28	0.38	23	2.09	58.48
N1677393105_1	2011-057T05:43:57.104	BL1	80.1	32.5	28	0.38	21	4.83	138.24
N1677393105_1	2011-057T05:43:57.104	BL1	80.1	32.5	28	0.38	21	4.00	128.48
N1677395433_1	2011-057T06:22:45.090	BL1	110.8	32.8	28	0.38	24	2.03	94.23
N1677396597_1	2011-057T06:42:09.082	BL1	111.0	33.1	28	0.38	21	1.46	65.34
N1677396597_1	2011-057T06:42:09.082	BL1	111.0	33.1	28	0.38	21	1.76	55.48
N1677428049_1	2011-057T15:26:20.884	BL1	44.0	32.1	28	0.38	20	3.07	86.72
N1677428049_1	2011-057T15:26:20.884	BL1	44.0	32.1	28	0.38	20	1.69	77.20
N1677432123_1	2011-057T16:34:14.858	BL1	76.4	30.8	28	0.38	19	1.10	41.40
N1677433869_1	2011-057T17:03:20.847	BL1	97.3	32.7	28	0.38	21	1.53	63.90
N1677434451_1	2011-057T17:13:02.843	BL1	112.8	32.8	28	0.38	23	3.75	92.18
Σ over storm	2011-057	BL1				1.9		22	
N1678130684_1	2011-065T18:36:51.234	BL1	123.7	32.6	39	0.82	19	8.29	187.43
N1678132407_1	2011-065T19:05:34.613	GRN	137.9	34.3	78	0.04	20	0.25	5.98

cloud particles' single scattering albedo from 1 to 0.95 does not substantially affect lightning obscuration (Dyudina et al., 2002). This tells us that we would probably see the lightning through the dense white clouds on Saturn if the lightning was there. It makes the cloud-blocking explanation for lightning non-detection less convincing.

Another explanation is that lightning simply does not occur directly under the bright clouds. Then the question arises as to where the lightning-producing updrafts deposit their cloud material. The bright clouds in the 2009 and 2011 storms are substantially higher than the levels producing lightning, and may be displaced from the thunderstorms by high-elevation winds like the anvils of terrestrial thunderstorms. In 2004 bright clouds were observed to appear correlated in time with intensification of SEDs (Dyudina et al., 2007). The time for the convective plumes to rise from the lightning-producing level in 2004 was less than a day. Assuming rise time $dt = 11$ h, the bright cloud will be displaced as it rises in the wind shear by $\Delta v_z/2 \cdot dt$, where Δv_z is the difference between the upper winds and deep winds at the lightning level. Δv_z was derived in Section 2. For 2004 $\Delta v_z = 6$ m s^{-1} and for 2011 $\Delta v_z = 13$ m s^{-1} the corresponding displacements $\Delta\ v_z/2 \cdot dt$ are ~100 and 250 km. This is too small to move the bright clouds at the storm's west edge as far away from the observed lightning as in Figs. 2–4, where the separation is about 5° longitude, or ~4000 km. Therefore, the 2011 lightning lacking corresponding dense clouds are likely produced in deep clouds not penetrating to the upper troposphere.

7.2. Lightning detection strategies

Optical detection of lightning on Saturn proved to be much more challenging than on Jupiter. The reason is not the difference in lightning, as both energies and flash rates of individual storms on Jupiter and Saturn are comparable (see Table 2). What makes Saturn's lightning hard to detect is statistics. First, there are many fewer storms on Saturn: two, one or none at a given time (Fischer et al., 2011b) compared to ~50 simultaneous storms at Jupiter (29 storms detected by Galileo per 0.6 × Jupiter's area surveyed (Dyudina et al., 2004)). Cassini's observations are planned years in advance. Saturn storms last less than a year (Fischer et al., 2011b). This makes it impossible for Cassini to specifically target Saturn's storms. As a result, Saturn's surveys are "blind" and the chances of seeing lightning are much lower than for Jupiter.

Second, it is much harder to obtain long survey times for Saturn because of the background ring-illuminated clouds. While Jupiter's night-side observations can be safely made with long exposures of several minutes, Saturn's ring-illuminated night side saturates the images much faster. As a result, many images are needed instead of one to get the same survey time. The extreme example of this is the 2011 dayside detection of Saturn's lightning. As can be seen in Fig. 10, only the extraordinary high flash rate of the 2011 storm made it possible to detect lightning in the short 1.9-s survey. Less frequent lightning, like in the 2009 storms, would not be detectable with such a short survey. Both 2009 data sets are exceptions from that long-survey problem due to the fortunate darkness of the edge-on illuminated rings near the equinox, which happens

once every ~15 years. As a result, several minute exposures were combined into longer surveys, which allowed lightning detection in 2009. An alternative strategy for long surveys would be just to take hundreds of short-exposure images instead of a few long-exposure ones. For Cassini, a large number of images, combined with the high spatial resolution required for lightning detection hit Cassini restrictions for data volume transmission to the Earth. However, our detections prove that lightning can be detected even on the day side of Saturn.

Remarkably, the weaker 2009 storms produce flashes with optical energies of the order 10^9 J, similar to the 2011 energies. The 2009 bright flashes would be detectable on the day side if Cassini was able to make long dayside surveys. Due to the much lower flash rates of 2009, thousands of images would be needed for detection in order to provide an appropriate survey time (tens of minutes) by adding up the short dayside image exposures.

Acknowledgments

This research was supported by the NASA Cassini Project. GF is supported by a Grant from the Austrian Science Fund FWF (P24325-N16).

Appendix A

A.1. Detailed properties of all detected optical flashes

Table A1 summarizes all lightning detected to date in Cassini images. The flashes are ordered chronologically. The names of the images in which they are seen are listed. The date is given using the day of the year ("day" in Table A1). The calendar dates are the following: 2009-229 is August 17 2009; 2009-334 is November 30 2009; 2011-057 is February 26 2011; 2011-065 is March 6 2011. The "time" is given in the format of (hours:minutes:seconds), where seconds are given to millisecond accuracy, and are separated by decimal point. The times quoted are the middles of the camera's exposures. The 2009 nightside images detected multiple flashes in some images. For 2009 several lines in the table with the same image name correspond to different flashes. The 2011 dayside images with much shorter exposures usually detected a single flash per image, except for the two flashes in the same image on 2011-057T04:45:45.

The flash brightness B was measured by subtracting background images which were close in time and contained no flash. In some cases, two different background images were used for subtraction. Except for the 2011-057T04:45:45 image, the 2011 pairs of lines in the table with the same image name correspond to the same flash but with different backgrounds subtracted, which gave different brightness estimates. The discrepancy between these two estimates gives a sense of uncertainties in our optical lightning energy values E_o in 2011, which is around $\pm 1 \times 10^9$ J. The average of the two estimates was used in all calculations. The lines labeled "Σ over storm" give the sum of all flash energies in each observation. Note that for 2011 storm it is not equal to the sum over the "E_o" column. The two different estimates for the same flash are shown in two lines but their average is added to the sum only once. The "filter" column indicates which filter was used by the Narrow Angle Camera, "CL1" is clear filter, "BL1" is blue, and "GRN" is green filter (filter details can be found in Porco et al. (2004)). Columns labeled "Lon" and "Lat" show west longitude and planetocentric latitude of the flashes, respectively. Note that during the long exposures, e.g., in 2009-229 observations, Saturn moved substantially underneath the camera, so the apparent longitudes listed in the table for the middle of exposure differ from the actual flash longitude by as much as 0.2°. Column "km/pix" shows the image scale in km, not accounting for slant-viewing foreshortening. For some of the images the pixels are binned in 2×2 or 4×4 pixel boxes onboard Cassini, and the image scale is 2 or 4 times coarser than the nominal camera scale. The "t_{exp}" column shows exposure time for individual images. For the "Σ over storm" lines the "t_{exp}" column gives the total survey time, which is discussed in Section 5. The emission angle e is shown as it was used for E_o calculation in Eq. (1). B is the peak brightness (compare to Figs. A1, A2, A3 of the Appendix A).

A.2. Lightning detection technique and survey times

Because the appearance of lightning flashes in dayside Cassini images can be confused with small sunlit clouds, the intermittent nature of lightning was used to verify the validity of our detections. Lightning does change between images taken tens of minutes apart. Sunlit clouds do not change on the timescales of tens of minutes, so the repeated images of the same area can be used for background subtraction to reveal lightning. Fig. A1 shows an example of such background subtraction, which had been applied to all of the images that we searched for lightning. Images taken tens of minutes apart differ in solar illumination due to Saturn's rotation. To compensate for that, we subtracted the smooth large-scale illumination gradient from the background image. Also the default navigation of the images has a random error of about 3–5 pixels. To compensate for that we imposed the set of few-pixel deviations from the default navigation to the latitude/longitude grid, and searched for the solution that minimizes the discrepancy between the images. As can be seen in the middle panel of Fig. A1, this

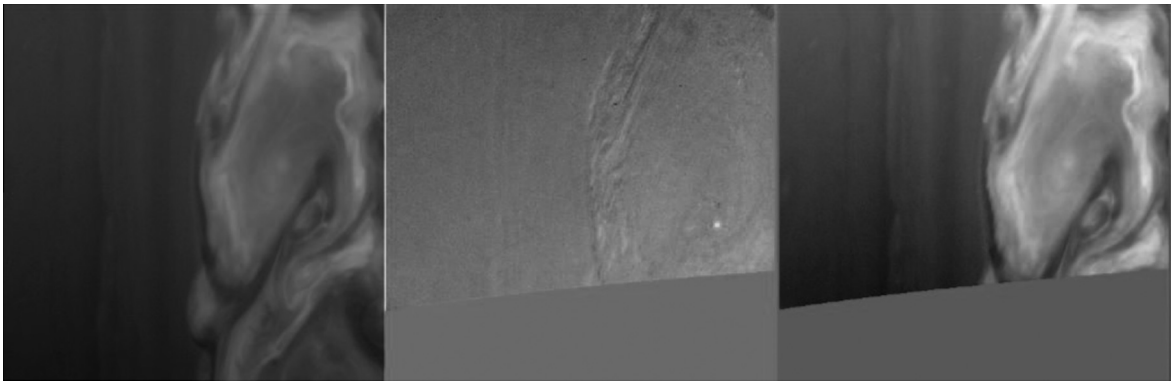

Fig. A1. Demonstration of image subtraction used to detect lightning. The left panel is the raw BL1 image from the camera taken at 2011-057T05:43:57 (see Table A1 of the Appendix A for flash details). The right panel is the BL1 image taken 10 min later reprojected to the same latitude/longitude grid as the left panel. Middle panel is the difference between the left and the right panel, stretched in brightness to bring up faint features.

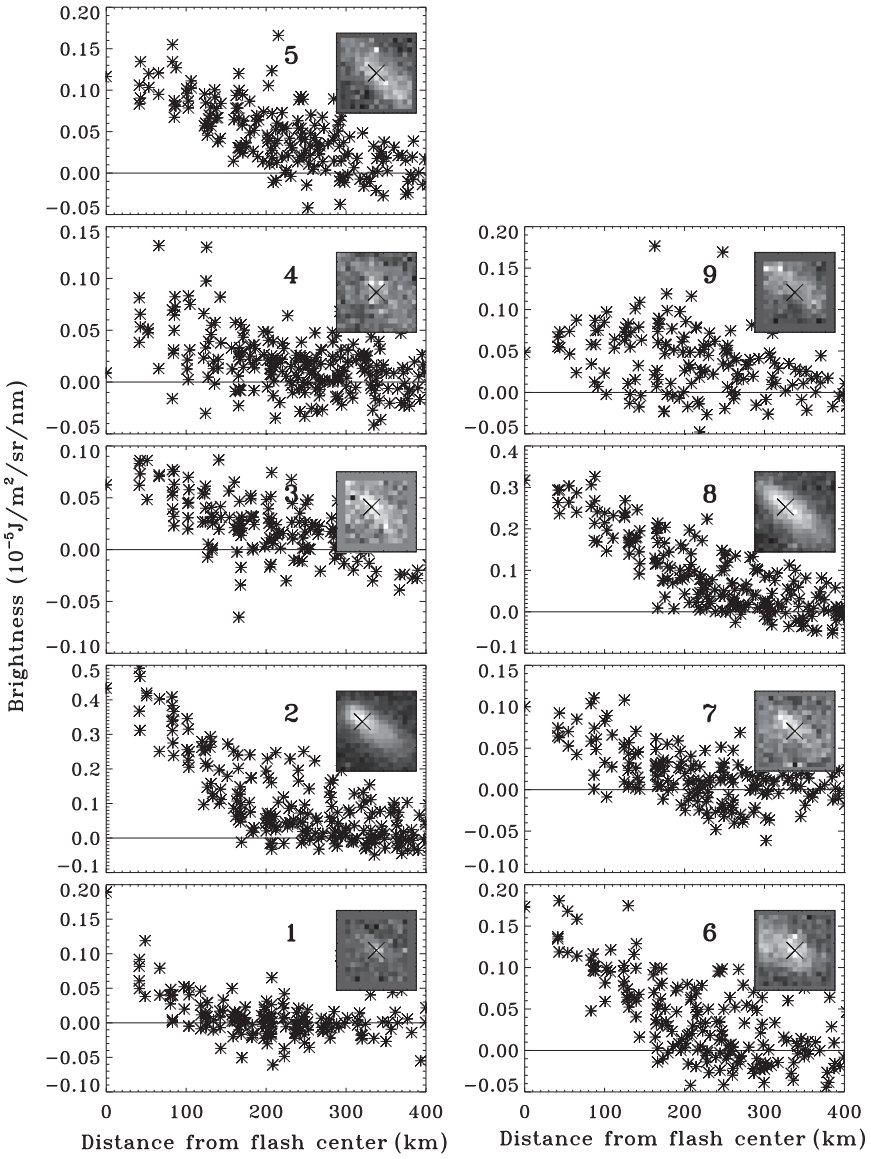

Fig. A2. Brightness distribution in the flashes observed during equinox (data for DOY 229 of 2009 in Table A1). See plot description in Fig. 7 of the main paper.

resulted in almost complete subtraction of the cloud features because the clouds did not move much in the time between the images. This technique allowed us to identify intermittent lightning like the one that appears as a bright spot on the right of the middle panel of Fig. A1.

All of the subsequent processing of the lightning flash images on the day side (brightness distribution studies and energy calculations) had been done after such background subtraction. Typically the second image with the same filter in the image sequence was used as a background for the first one. Then the third image was subtracted from the second one and so on. For the brightness measurements, some of image pairs were subtracted in reverse order such that the lightning always appears positive even if it is detected as a bright spot in the second image.

The survey time for February 26 2011 observations in Section 4 was calculated accounting for only the overlapping parts of the images. Namely, the location of the storm is considered to be "covered by the image" only when a pair of the images covers that location, such that the background subtraction can be done. Only the difference images can be searched for lightning, and thus, only the overlapping image areas were accounted for in the lightning survey. The survey time for all parts of the storm is very similar because the images were taken regularly every ~10 min as Saturn rotates underneath Cassini, covering the storm homogeneously with 2–3 overlapping images during each of the 5-h observations in Fig. A2. Accordingly, we can give a single survey time of 1.9 s which applies to all parts of the storm. This is equivalent to the survey of the whole 27-image-wide storm in 1.9 s.

A.3. Wind and vorticity measurements

The velocity and vorticity measurements were made using pairs of NAC observations of the storm taken 10 min apart. Each observation was photometrically calibrated using the Cisscal program (West et al., 2010). Then simple cylindrical maps were made using the navigation tool Vicar (http://www-mipl.jpl.nasa.gov/PAG/public/vug/vugfinal.html). Wind speeds were determined from cloud motions measured with an automatic wind tracker (Tracker3, also in Vicar). Consecutive 10-min pairs of observations overlapped in part and the overlapping regions were compared to confirm that the measurements were consistent. The limb of the planet was not visible in these observations, making navigation

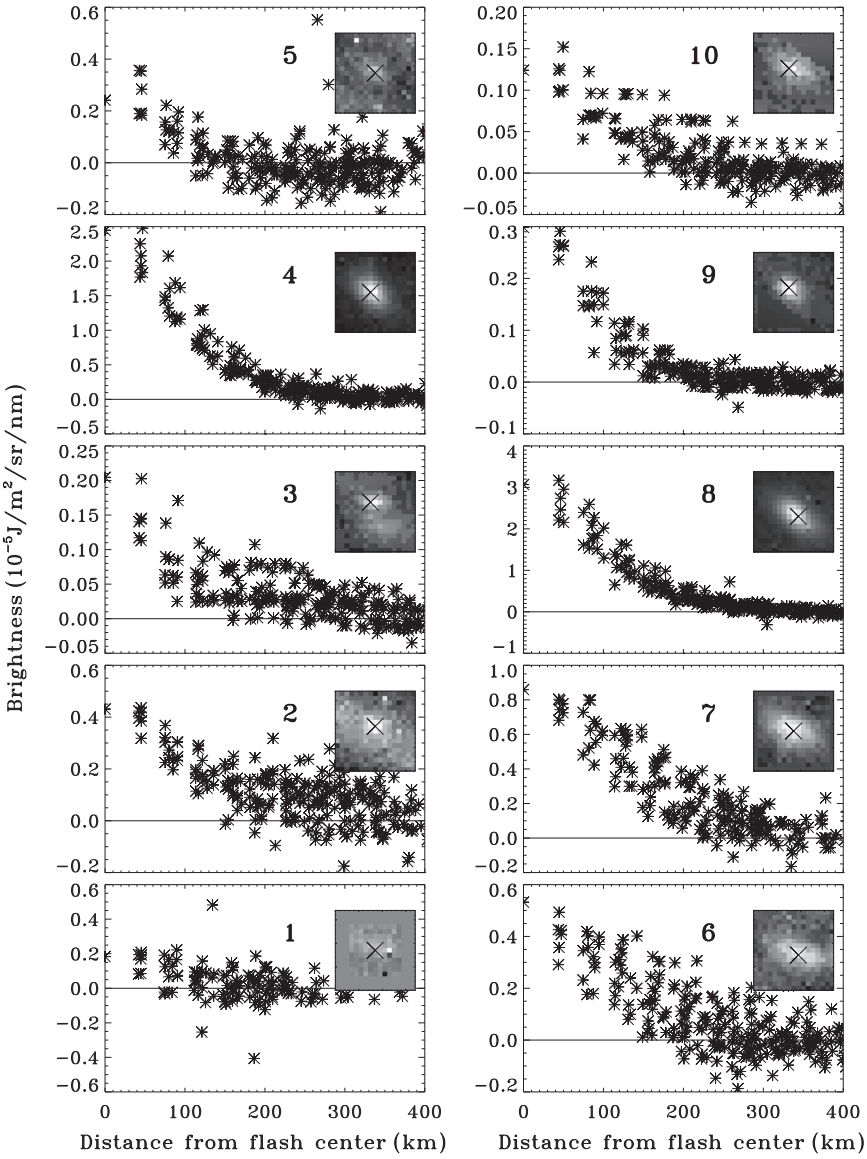

Fig. A3. Brightness distribution in the flashes on DOY 334 of 2009 (see Table A1). See plot description in Fig. 7 of the main paper.

complicated. We used Vicar to make simple cylindrical maps based on the default pointing of the spacecraft, then measured the apparent motion of the overall scene or of the slowest moving clouds in a pair of maps. Those motions were easily distinguished from real advection because they imply impossible motion, such as the entire storm being displaced by large distances in latitude almost instantaneously. These motions were resolved into camera rotations and a small rotation was applied to the camera pointing for compensation.

In Figs. 3–5 each map is a mosaic of 27 images in each filter, taken at 10 min intervals and overlapping each other by 2/3 of an image. Velocity and vorticity were determined by tracking clouds in the overlap regions. The overlap regions themselves overlap, which allows complete measurement of the velocity field with no gaps in longitude. Thus we have two independent measurements of the velocity and vorticity fields – one from the first mosaic and one from the second. Pairs of images taken 11 h apart were not used because the small-scale features became unrecognizable over that time interval. The measurements of velocity are done relative to the centerline of the storm and not relative to the reference frame of Saturn.

There are two main sources of uncertainty in using cloud displacements to measure winds – feature tracking and camera pointing. Feature tracking involves finding the best correlation between two boxes – square arrays of pixels – one from the first image and one from the second image. Sub-pixel precision is possible in the best cases, e.g., when the features do not change shape during the time between images. The short time interval leads to higher precision, because the features do not have time to change. Still higher precision is obtained by taking a bigger box, but that sacrifices spatial resolution. In these studies we used a correlation box of 31 × 31 pixels, which is 465 km on a side. The velocity vectors are plotted on a grid of 15 pixels, which is 225 km on a side. A rough estimate of the precision of each velocity measurement is ±5 m s^{-1}.

The error in camera pointing adds a constant unknown displacement to all the pixels in a given image. The error is independent of the time interval, so the resulting error in velocity is greatest when the time interval is short. This effect is the opposite of that associated with feature tracking. For these observations, the camera pointing uncertainty is ∼5 pixels, or ∼75 km. That number, divided by 10 min, is a velocity of 125 m s^{-1}, which is as large as

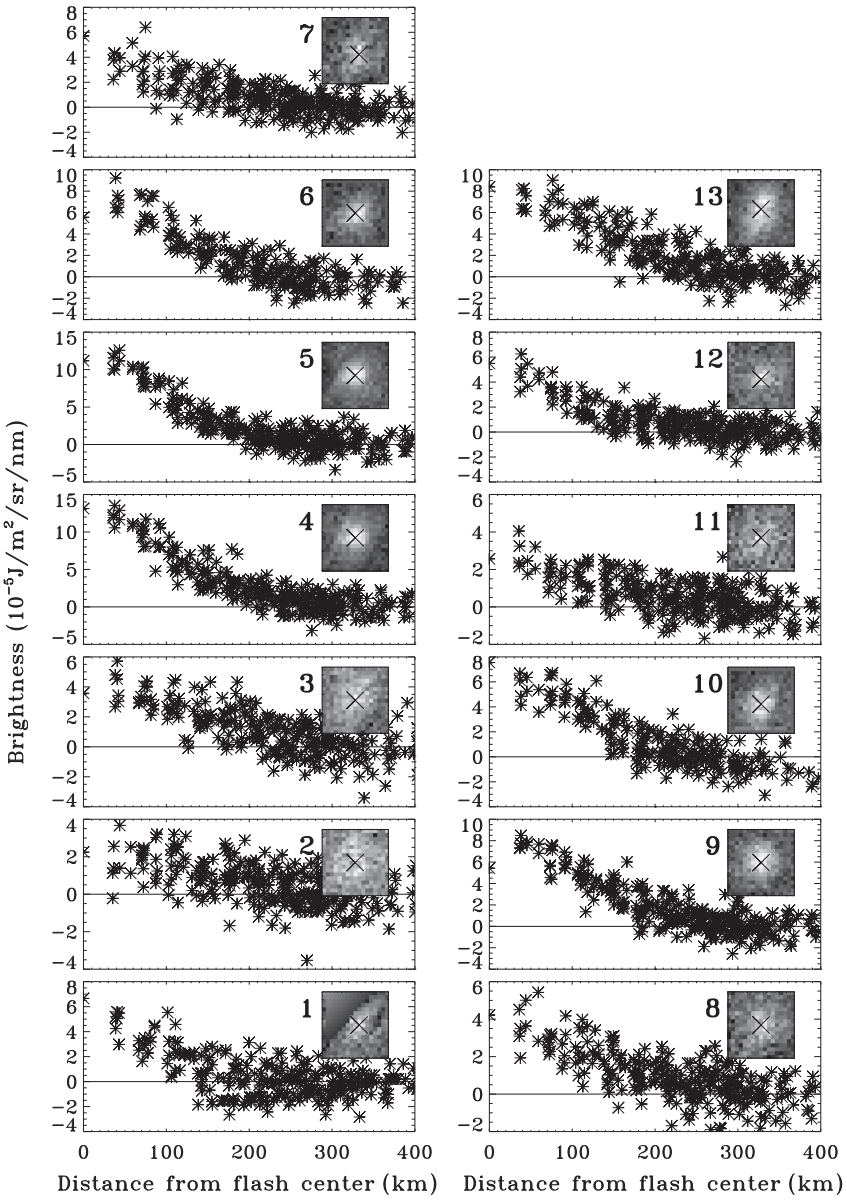

Fig. A4. Brightness distribution in the flashes on DOY 57 of 2011 (see Table A1). See plot description in Fig. 7 of the main paper.

the largest velocities we are measuring. Therefore to produce the velocity and vorticity maps of Figs. 3–5, we adjusted the pointing of one image so that certain features had the same latitudes and longitudes as in the other image. In other words, we forced these features to have zero velocity. Since our longitude system rotates with the head, we chose features on the central latitude of the storm in the hope that those features were moving with the head. It is difficult to estimate the error in this procedure. The best estimate is probably to compare the measurements from the two maps taken 11 h apart. Although the large-scale features do change, the velocity and vorticity fields are quite similar. Nevertheless, one should regard the maps as measurements of velocity relative to the centerline of the storm and not as absolute velocity.

Since vorticity is a derivative of velocity, it is much less affected by errors of camera pointing, which adds a near-constant offset to all velocities obtained from a given pair of images. But rather than take derivatives directly, we used Stokes theorem by taking line integrals around closed circuits within the velocity map. Again there was a compromise between lowering the spatial resolution with large circuits and producing a noisy product with small circuits. We finally settled on circuits that had five velocity pixels on a side. Since one pixel in the velocity map is 225 km, the resolution of the vorticity map is ~1000 km. Vorticity on smaller scales is lost during this procedure.

A.4. Brightness calibration B

Cassini images are routinely calibrated into the units of photon s^{-1} cm^{-2} sr^{-1} nm^{-1} (West et al., 2010). To compare instantaneous flashes detected with different exposure times, we multiply the calibration by the exposure. We obtain wavelength-normalized brightness B in units of J m^{-2} sr^{-1} nm^{-1} from the standard calibration assuming the photons' energy is $h\,c/\lambda$, where h is the Planck constant, c is the speed of light, and the wavelengths are $\lambda = 651$ and $\lambda = 455$ nm for clear and blue filters, respectively. The unit of brightness B, which we define here, is different from commonly used unit of intensity because it is related to the energy accumulated over the exposure time instead of power (emitted per unit time), and also because it is normalized by wavelength.

A.5. Non-traditional use of term "SED" in this paper

We use term "SEDs" non-traditionally. The SED data points in Fig. 8 are single RPWS measurements taken at the temporal resolution of 35 ms. In previous publications, e.g., Fischer et al. (2007), consecutive data points are combined into longer-duration continuous signals, with a typical duration of 70 ms, or two 35-ms measurements. These longer-duration signals were termed "SEDs", and the single measurements at a certain time and frequency were called "SED pixels". The longer-duration SEDs often overlap in time in the stronger 2010–2011 storm and cannot be confidently separated. To avoid confusion, we do not group single SED measurements in this paper. We call single measurements "SEDs" instead of "SED pixels".

A.6. Optical and radio detection limits

The intensity of SEDs and the detectability of optical flashes depend on Saturn–Cassini distance, which is usually measured in Saturn's radii R_S. All three sets of observations were taken from a similar distance ($35R_S$ for August 2009, $42R_S$ for November 2009, and $42R_S$ for February 2011). For the RPWS instrument, this leads to similar detection efficiencies resulting in almost the same minimum SED power around 1 W/Hz in Fig. 10. SEDs with lower radio powers are most likely present, but cannot be detected since their radiated power is below the galactic background. The situation is different for the optical detection efficiency since the three sets of observations were taken in different conditions. The nightside observations from August 2009 and November 2009 have a similar minimum in optical energy of $\sim 2 \times 10^8$ J with the exception of one flash with just $\sim 1 \times 10^8$ J detected in August 2009. This is a single-pixel flash (Table 1 and Fig. 2 in the Appendix A), and thus may be a cosmic ray hit on the detector not related to lightning. Fig. 10 clearly shows that the dayside flash observations from February 2011 were able to detect only flashes with optical energies $>1.0 \times 10^9$ J, at a rate of $\sim$5 per second, although flashes with lower energies should exist with higher rates, e.g., at $\sim$10 per second detected by RPWS. The optical rate of $\sim$5 per second corresponds to the average of two SEDs per optical flash. The two 35-ms-long SEDs per lightning flash is also derived from the average $\sim$70-ms duration of the continuous multiple-SED signals (Fischer et al., 2007). This suggests that the 2011 flashes are as easy to detect with RPWS as with the camera. In November 2009 RPWS detected about 0.2 flashes per second, but the camera detected only about 0.02 flashes per second (Fig. 10), which probably means that radio observations are more sensitive, especially to low-energy lightning. The terrestrial observations by the FORTE satellite found that only 50% of all intracloud events detected in the HF radio range had an optical counterpart (Light et al., 2001). The optical scattering can be highly variable due to the event's placement in the cloud, the cloud optical depth and the viewing angle. Note that we have not detected any optical flash with no radio counterpart when the RPWS instrument was listening (Figs. 8 and 9). The detection efficiency of RPWS and ISS is probably similar for high-energy lightning. This has led to similar flash and SED rates for the 2011 storm, and Figs. 8 and 9 show that each high intensity SED (>30 W/Hz) has resulted in an optical detection when ISS was taking an image.

A.7. Additional images on flash appearance

Figs. A2, A3, A4 show the appearance, size, brightness distribution, and demonstrate the noise level in the detected flashes. The panels are labeled in chronological order according to Table A1 of the Appendix A.

In our estimate of the lightning spot size we did not account for the camera's point spread function (PSF). We believe the effect of PSF is not large on the lightning spots which are 5–10 pixels across. Also, PSF effect was not accounted for in previous studies (Little et al., 1999; Dyudina et al., 2002, 2007, 2010).

Appendix B. Supplementary material

Supplementary data associated with this article can be found, in the online version, at http://dx.doi.org/10.1016/j.icarus.2013.07.013.

References

Baines, K.H. et al., 2007. Polar lightning and decadal-scale cloud variability on Jupiter. Science 318, 226–229.

Baines, K.H. et al., 2009. Storm clouds on Saturn: Lightning-induced chemistry and associated materials consistent with Cassini/VIMS spectra. Planet. Space Sci. 57, 1650–1658.

Borucki, W.J., McKay, C.P., 1987. Optical efficiencies of lightning in planetary atmospheres. Nature 328, 509–510.

Borucki, W.J., Bar-Nun, A., Scarf, F.L., Cook, A.F., Hunt, G.E., 1982. Lightning activity on Jupiter. Icarus 52, 492–502.

Burns, J.A., Showalter, M.R., Cuzzi, J.N., Durisen, R.H., 1983. Saturn's electrostatic discharges: Could lightning be the cause? Icarus 54, 280–295.

Christian, H.J., Goodman, S.J., 1987. Optical observations of lightning from a high-altitude airplane. J. Atmos. Oceanic Technol. 4, 701–711.

Dyudina, U.A., Ingersoll, A.P., Vasavada, A.R., Ewald, S.P., 2002. Monte Carlo radiative transfer modeling of lightning observed in Galileo images of Jupiter. Icarus 160, 336–349.

Dyudina, U.A., del Genio, A.D., Ingersoll, A.P., Porco, C.C., West, R.A., Vasavada, A.R., Barbara, J.M., 2004. Lightning on Jupiter observed in the H_α line by the Cassini imaging science subsystem. Icarus 172, 24–36.

Dyudina, U.A., Ingersoll, A.P., Ewald, S.P., Porco, C.C., Fischer, G., Kurth, W., Desch, M., Del Genio, A., Barbara, J., Ferrier, J., 2007. Lightning storms on Saturn observed by Cassini ISS and RPWS during 2004–2006. Icarus 190, 545–555.

Dyudina, U.A. et al., 2010. Detection of visible lightning on Saturn. Geophys. Res. Lett. 37, L09205.

Farrell, W.M., Kaiser, M.L., Fischer, G., Zarka, P., Kurth, W.S., Gurnett, D.A., 2007. Are Saturn electrostatic discharges really superbolts? A temporal dilemma. Geophys. Res. Lett. 34, L06202.

Fischer, G., Kurth, W.S., Dyudina, U.A., Kaiser, M.L., Zarka, P., Lecacheux, A., Ingersoll, A.P., Gurnett, D.A., 2007. Analysis of a giant lightning storm on Saturn. Icarus 190, 528–544.

Fischer et al., 2006a. On the intensity of Saturn lightning. In: Rucker, H.O., Kurth, W.S., Mann, G. (Eds.), Planetary Radio Emissions VI. Austrian Academy of Sciences Press, Vienna, pp. 123–132.

Fischer et al., 2006b. Saturn lightning recorded by Cassini/RPWS in 2004. Icarus 183, 135–152.

Fischer et al., 2011a. A giant thunderstorm on Saturn. Nature 475, 75–77.

Fischer et al., 2011b. Overview of Saturn lightning observations. In: Rucker, H.O., Kurth, W.S., Louarn, G., Fischer, P. (Eds.), Planetary Radio Emissions VII. Austrian Academy of Sciences Press, Vienna, pp. 135–144.

Fletcher, L.N. et al., 2011. Thermal structure and dynamics of Saturn's northern springtime disturbance. Science 332, 1413–1417.

Gierasch, P.J. et al., 2000. Observation of moist convection in Jupiter's atmosphere. Nature 403, 628–630.

Gurnett, D.A. et al., 2004. The Cassini radio and plasma wave investigation. Space Sci. Rev. 114, 395–463.

García-Melendo, E., Hueso, R., Sánchez-Lavega, A., Legarreta, J., del Río-Gaztelurrutia, T., Pérez-Hoyos, S., Sanz-Requena, J.F., 2013. Atmospheric dynamics of Saturn's 2010 giant storm. Nature Geoscience 6, 525–529.

Hanel, R.A., Conrath, B.J., Kunde, V.G., Pearl, J.C., Pirraglia, J.A., 1983. Albedo, internal heat flux, and energy balance of Saturn. Icarus 53, 262–285.

Holton, J.R., 2004. An Introduction to Dynamic Meteorology. fourth ed. Elsevier Academic Press, Amsterdam.

Houze, R.A., 1993. Cloud dynamics. International Geophysics Series, vol. 53. Academic Press, London.

Ingersoll, A.P., Gierasch, P.J., Banfield, D., Vasavada, A.R.and the Galileo Imaging Team, 2000. Moist convection as an energy source for the large-scale motions in Jupiter's atmosphere. Nature 403, 630–632.

Ingersoll, A.P., Dyudina, U.A., Ewald, S.P., 2013. Mesoscale waves in Saturn's 2010–2011 lightning storm. Icarus, submitted for publication.

Janssen, M.A., Ingersoll, A.P., Allison, M., Gulkis, S., Laraia, A.L., Baines, K.H., Edgington, S.G., Kelleher, K., Oyafuso, F., 2013. Saturn's thermal emission at 2.2-cm wavelength as imaged by the Cassini RADAR radiometer. Icarus, 226, 522–535.

Kaiser, M.L., Connerney, J.E.P., Desch, M.D., 1983. Atmospheric storm explanation of saturnian electrostatic discharges. Nature 303, 50–53.

Laraia, A.L., Ingersoll, A.P., Janssen, M.A., Gulkis, S., Oyafuso, F., Allison, M., 2013. Analysis of Saturn's thermal emission at 2.2 cm wavelength: Spatial distribution of ammonia vapor. Icarus, 226, 641–654.

Lewis, E.A., 1982. High frequency radio noise. In: CRC Handbook of Atmospherics, vol. 1, pp. 251–288.

Lewis, J.S., 1980. Lightning on Jupiter: Rate, energetics, and effects. Science 210, 1351–1352.
Light, T.E., Suszcynsky, D.M., Kirkland, M.W., Jacobson, A.R., 2001. Simulations of lightning optical waveforms as seen through clouds by satellites. J. Geophys. Res. 106, 17103–17114.
Little, B., Anger, C.D., Ingersoll, A.P., Vasavada, A.R., Senske, D.A., Breneman, H.H., Borucki, W.J. and the Galileo SSI Team, 1999. Galileo images of lightning on Jupiter. Icarus 142, 306–323.
Oliver, J.E., 2005. The Encyclopedia of World Climatology (Encyclopedia of Earth Sciences Series). Springer.
Piepgrass, M.V., Krider, E.P., Moore, C.B., 1982. Lightning and surface rainfall during Florida thunderstorms. J. Geophys. Res. 87, 11193–11202.
Porco, C.C. et al., 2003. Cassini imaging of Jupiter's atmosphere, satellites, and rings. Science 299, 1541–1547.
Porco, C.C. et al., 2004. Cassini imaging science: Instrument characteristics and anticipated scientific investigations at Saturn. Space Sci. Rev. 115, 363–497.
Porco, C.C. et al., 2005. Cassini imaging science: Initial results on Saturn's atmosphere. Science 307, 1243–1247.
Salby, M.L., 1996. Fundamentals of Atmospheric Physics. Academic Press, Inc., San Diego.
Sánchez-Lavega, A. et al., 2011. Deep winds beneath Saturn's upper clouds from a seasonal long-lived planetary-scale storm. Nature 475, 71–74.
Sayanagi, K.M., Dyudina, U.A., Ewald, S.P., Fischer, G., Ingersoll, A.P., Kurth, W.S., Muro, G.D., Porco, C.C., West, R.A., 2013. Dynamics of Saturn's great storm of 2010–2011 from Cassini ISS and RPWS. Icarus 223, 460–478.
Thomason, L.W., Krider, E.P., 1982. The effects of clouds on the light produced by lightning. J. Atmos. Sci. 39, 2051–2065.
Tomasko, M.G., Doose, L.R., 1984. Polarimetry and photometry of Saturn at from Pioneer 11: Observations and constraints on the distribution and properties of cloud and aerosol particles. Icarus 58, 1–34.
Turman, B.N., 1978. Analysis of lightning data from the DMSP satellite. J. Geophys. Res. 83, 5019–5024.
Uman, M.A., 1987. The Lightning Discharge. Academic Press, New York.
Volland, H., 1982. Low frequency radio noise. In: CRC Handbook of Atmospherics, vol. 1, pp. 179–250.
West, R. et al., 2010. In-flight calibration of the Cassini imaging science sub-system cameras. Planet. Space Sci. 58, 1475–1488.
Yair, Y., Fischer, G., Simões, F., Renno, N., Zarka, P., 2008. Updated review of planetary atmospheric electricity. Space Sci. Rev. 137, 29–49.